

## Multiscale Models for Cumulus Cloud Dynamics

SAMUEL N. STECHMANN\*

*Department of Mathematics, and Department of Atmospheric and Oceanic Sciences,  
University of California, Los Angeles, Los Angeles, California*

BJORN STEVENS

*Max-Planck-Institut für Meteorologie, Hamburg, Germany, and Department of  
Atmospheric and Oceanic Sciences, University of California,  
Los Angeles, Los Angeles, California*

(Manuscript received 13 November 2009, in final form 7 May 2010)

### ABSTRACT

Cumulus clouds involve processes on a vast range of scales—including cloud droplets, turbulent mixing, and updrafts and downdrafts—and it is often difficult to determine how processes on different scales interact with each other. In this article, several multiscale asymptotic models are derived for cumulus cloud dynamics in order to (i) provide a systematic scale analysis on each scale and (ii) clarify the nature of interactions between different scales. In terms of scale analysis, it is shown that shallow cumulus updrafts can be described by balanced dynamics with a balance between source terms and ascent/descent; this is a cloud-scale version of so-called weak-temperature-gradient models. In terms of multiscale interactions, a model is derived that connects these balanced updrafts to the fluctuations within the balanced updraft envelope. These fluctuations describe parcels and updraft pulses, and this model encompasses some of the multiscale aspects of entrainment. In addition to this shallow cumulus model, to provide a broad picture of general cumulus dynamics, multiscale models are also derived for other scales; these include models for parcels and subparcel turbulent mixing and models for deep cumulus. Broadly speaking, the differences between the shallow and deep cases convey the notion that shallow cumulus dynamics are parcel dominated, whereas deep cumulus dynamics are updraft dominated; this is largely due to the difference in the apparent magnitude of the background temperature stratification. In addition to their use in guiding theory, the multiscale models also provide a framework for multiscale numerical simulations.

### 1. Introduction

Cumulus clouds involve physical processes on a vast range of scales, all of which are important for a cloud's development. These include aerosols and cloud droplets on scales smaller than  $10^{-3}$  m, turbulent motions on scales of roughly 1 m within the cloud, updrafts on scales of roughly  $10^3$  m, and the ambient environment in which the cloud forms. Because of this wide range of scales, clouds remain poorly understood and thus contribute

greatly to uncertainty in predictions of weather and climate (Houghton et al. 2001; Moncrieff et al. 2007; Bodenschatz et al. 2010). A growing body of evidence suggests that in order to fully understand cloud dynamics and their role in climate systems, the physical processes operating on each scale must be accounted for together (Albrecht 1989; Stevens and Brenguier 2009). In other words, not only must each process on each scale be understood, but the interactions across scales must also be understood. Here we approach this problem by designing multiscale models.

One example of a multiscale process in clouds is the entrainment of ambient air parcels into a cloud updraft (Blyth 1993; Houze 1993; Stevens 2005). This involves the interaction between a large-scale updraft envelope and the smaller-scale fluctuations within it: the dynamics of the updraft envelope can potentially promote entrainment, and the cumulative effects of many entrainment

---

\* Current affiliation: Department of Mathematics, University of Wisconsin—Madison, Madison, Wisconsin.

---

*Corresponding author address:* Samuel Stechmann, Department of Mathematics, University of Wisconsin—Madison, 480 Lincoln Dr., Madison, WI 53706.  
E-mail: stechmann@wisc.edu

events can potentially affect the larger-scale updraft. Important aspects of the entrainment process have been documented in numerical simulations of clouds (Grabowski and Clark 1991, 1993a,b; Carpenter et al. 1998a,b,c). However, many uncertainties remain about this multiscale process and its role in cloud development, such as the relative roles of entrainment at cloud top versus lateral boundaries (Blyth 1993; Heus and Jonker 2008).

Another example of a multiscale process in clouds is the interaction between turbulent mixing and cloud droplet evolution. For instance, when a parcel of ambient air is entrained into a cloud, the turbulent mixing of the ambient and cloudy air eventually leads to evaporation of cloud liquid water. The final droplet distribution at the end of the mixing event depends crucially on the relative time scales of the mixing and evaporation (Baker et al. 1984; Su et al. 1998; Burnet and Brenguier 2007; Andrejczuk et al. 2009). In addition to evaporation of droplets, collisions of droplets can also be influenced, and possibly enhanced, by turbulent fluid motions (Shaw 2003; Xue et al. 2008). Not only are these topics important for our theoretical understanding of clouds, but they are also important for numerical cloud models, in which such processes are not explicitly resolved but could potentially be included as a subgrid-scale parameterization (Grabowski 2007; Morrison and Grabowski 2008).

A great deal has been learned about these cloud processes through different types of models of various complexities. Some of the simplest settings for understanding cloud processes are parcel models and column models (Rogers and Yau 1989; Houze 1993). While they have been in use for at least several decades, they continue to provide new, useful insight into cloud processes (Stevens and Seifert 2008; Seifert and Stevens 2010). One drawback of parcel and column models is that they only represent dynamics on a single scale (i.e., the scales of parcels or columns) and must parameterize (or simply neglect) many important processes, such as entrainment and turbulent mixing. On the other hand, instead of simplified models, more complex numerical cloud models such as large-eddy simulations can represent three-dimensional fluid dynamics and are useful for understanding entrainment and cloud dynamics (Sommeria 1976; Stevens et al. 2001; Siebesma et al. 2003). However, it is often difficult to understand the important interactions across all scales in a three-dimensional simulation, and the vast range of scales makes these simulations computationally expensive. Furthermore, even though a vast range of scales is resolved, many important cloud processes must be parameterized. It is a major challenge to properly couple the resolved and unresolved processes, such as resolved fluid dynamics and unresolved

cloud microphysics; perhaps equally importantly, it is a major challenge to properly couple unresolved processes with each other, such as the effect of unresolved turbulent mixing on the parameterized microphysics (Grabowski 2007; Morrison and Grabowski 2008). A proper representation of all relevant processes, resolved and unresolved, might require a multiscale approach to cloud modeling.

The discussion above demonstrates the need for a better understanding of interactions between cloud processes on different scales. A useful mathematical tool for this is multiple scales asymptotics (Kevorkian and Cole 1996; Klein 2000; Majda 2003; Klein 2010). This method allows one to identify the equations governing different scales of interest, and, equally importantly, it also identifies the form of the interactions between the different scales. An example of the utility of multiple scales asymptotics is the work of Majda and Klein (2003), which identifies interactions on much larger scales in the tropics between synoptic-scale waves and intraseasonal/planetary-scale motions such as the Madden-Julian oscillation (Madden and Julian 1971). Subsequent work with multiscale models on these scales has shown how the synoptic-scale waves can interact with the Madden-Julian oscillation and, for instance, drive its westerly wind burst (Biello and Majda 2005; Majda and Stechmann 2009).

The main purpose of the present paper is to develop multiscale asymptotic models for cumulus cloud dynamics to (i) provide a systematic scale analysis on each scale and (ii) clarify the nature of interactions between different scales. For example, given a typical scaling for cumulus updrafts, is there a simplified dynamics that describes them? And what are the dominant interactions between updrafts and parcels? Besides their use for theoretical understanding, the models derived here also provide a framework for multiscale numerical simulations of clouds, which has already been shown to be a useful, promising technique for simulations of larger-scale atmospheric circulations (Grabowski 2001; Randall et al. 2003; Majda and Stechmann 2009).

The paper is organized as follows. In section 2, the framework of multiple scales asymptotics is reviewed. In section 3, a multiscale model for shallow cumulus dynamics is presented for the scales of updrafts and the parcels within them. To provide both detailed and general views of multiscale cumulus dynamics, this updraft/parcel model is discussed in detail, and models for other scales of cumulus dynamics are compared and contrasted in sections 4 and 5. In section 4 a multiscale model is presented for the scales of shallow cumulus parcels and subparcel turbulent mixing, and in section 5 the deep cumulus analogs of the shallow cumulus models are

presented. Conclusions and future directions are summarized in section 6.

## 2. Scaling

The equations for atmospheric fluid dynamics used as a starting point here are the dimensional Boussinesq equations:

$$\begin{aligned} \frac{D\mathbf{u}}{Dt} &= -\nabla p + \mathbf{k}g\left(\frac{\theta}{\theta_0} + \bar{\epsilon}q_v - q_c\right), \\ \frac{D\theta}{Dt} + \Gamma^\theta w &= \frac{L_v}{c_p} C, \\ \frac{Dq_v}{Dt} + \Gamma^q w &= -C, \\ \frac{Dq_c}{Dt} &= C, \quad \text{and} \\ \nabla \cdot \mathbf{u} &= 0, \end{aligned} \tag{1}$$

where

$$\frac{D}{Dt} = \frac{\partial}{\partial t} + \mathbf{u} \cdot \nabla = \frac{\partial}{\partial t} + u \frac{\partial}{\partial x} + v \frac{\partial}{\partial y} + w \frac{\partial}{\partial z},$$

$\mathbf{x} = (x, y, z)$  and  $\mathbf{u} = (u, v, w)$  are the spatial coordinates and velocities, and  $\nabla = (\partial_x, \partial_y, \partial_z)$  is the gradient. The vector  $\mathbf{k}$  denotes the unit vector in the upward vertical direction. The potential temperature  $\theta$  and water vapor mixing ratio  $q_v$  here are anomalies from background states  $\theta_0 + \Gamma^\theta z$  and  $q_{v,0} + \Gamma^q z$ , where linear dependence on  $z$  is used here for simplicity. The pressure here has a constant density factor  $\rho_0$  absorbed into it, and  $\bar{\epsilon} + 1$  is the ratio of the ideal gas constants for water vapor and dry air. Molecular diffusion terms have been left off the equations because we do not anticipate closing them on scales where such processes become relevant. The mixing ratio of condensed water is  $q_c$ , and the source term  $C$  represents condensation (or evaporation). The potential temperature source term should be multiplied by a factor of  $\theta/T$ , where  $T$  is temperature, but we leave it out above because this factor is set to unity here (and we use the notation  $T$  as a time variable in the rest of the paper). Strictly speaking the use of the Boussinesq equations is only valid for scales much shallower than an atmospheric-scale height. For applications involving deep convection, an anelastic model should be used instead of a Boussinesq model. Hence our use of these equations for deep convection is illustrative, done mostly to highlight distinctions between shallow and deep convection that are not sensitive to this assumption.

In its present form, (1) is technically only valid for nonprecipitating shallow convection, with closure for  $C$  pending. An attractive option for the source term is the

approach taken by Klein and Majda (2006), in which a warm rain microphysics closure is chosen and detailed asymptotics are worked out for the closure and for the thermodynamic background state. Here, the type of detailed analysis done by Klein and Majda (2006) is not repeated, but the moist thermodynamic scaling is motivated by their analysis and observations and simulations. In the spirit of Majda and Klein (2003) and Majda (2007), a generic source term is used rather than a specific condensation closure, and we then seek the multi-scale dynamics consistent with this scaling.

To nondimensionalize the equations above, the scales of shallow cumulus parcels are used here as the basic reference scales:

$$u_{\text{ref}} = 3.3 \text{ m s}^{-1}, \quad x_{\text{ref}} = 100 \text{ m}, \quad \text{and} \quad t_{\text{ref}} = 30 \text{ s},$$

where the components of space  $\mathbf{x}$  and velocity  $\mathbf{u}$  are scaled isotropically. Table 1 summarizes all of the reference values, which are based on a combination of observations, simulations, and theory. The values  $u_{\text{ref}} = 3.3 \text{ m s}^{-1}$  and  $x_{\text{ref}} = 100 \text{ m}$  represent a typical velocity fluctuation and length scale of a cloud parcel, and the time scale is the advective time scale. The potential temperature scale is chosen so that the reference buoyancy acceleration and parcel acceleration are in balance as  $\theta_{\text{ref}} = \theta_0 u_{\text{ref}} / g t_{\text{ref}} \approx 3.3 \text{ K}$ , and the reference heating rate is then  $\theta_{\text{ref}} / t_{\text{ref}} = 3.3 \text{ K (30 s)}^{-1}$ . The reference moisture scale is chosen so that the reference condensation rate and heating rate are in balance as  $q_{\text{ref}} = \theta_{\text{ref}} c_p / L_v \approx 1.3 \text{ g kg}^{-1}$ . Besides this motivation based on balances, these values are also consistent with typical parcel-scale fluctuations seen in observations and simulations (Rogers and Yau 1989; Houze 1993; Stevens et al. 2001; Siebesma et al. 2003; Stevens 2005). The reference background stratifications are taken as typical environmental lapse rates of

$$\Gamma_{\text{ref}}^\theta = \frac{3.3 \text{ K}}{1 \text{ km}} \quad \text{and} \quad \Gamma_{\text{ref}}^q = \frac{1.3 \text{ g kg}^{-1}}{1 \text{ km}}. \tag{2}$$

These reference values are most appropriate for trade wind cumulus but are applicable to other regimes to the extent that they are order-of-magnitude values. For instance, the value  $q_{\text{ref}} \approx 1.3 \text{ g kg}^{-1}$  can represent an order-of-magnitude range of  $\sim 0.4\text{--}4 \text{ g kg}^{-1}$ , and this value seems reasonable in the sense that  $0.13 \text{ g kg}^{-1}$  is probably too small and  $13 \text{ g kg}^{-1}$  is probably too large for a reference value for parcel-scale fluctuations. One could expect to see fluctuations of  $\sim 0.4\text{--}4 \text{ g kg}^{-1}$  due to fluctuations in the condensation rate and to mixing of cloudy and cloud-free air.

Using these reference scales to nondimensionalize (1), the equations become

TABLE 1. Reference scales for the shallow cumulus models.

Parameter	Derivation	Value	Description
$u_{\text{ref}}$	—	3.3 m s <sup>-1</sup>	Reference velocity scale
$x_{\text{ref}}$	—	100 m	Reference length scale
$t_{\text{ref}}$	$x_{\text{ref}}/u_{\text{ref}}$	30 s	Reference time scale
$\theta_0$	—	300 K	Surface potential temperature
$p_0$	—	10 <sup>5</sup> Pa	Surface pressure
$\rho_0$	—	1.2 kg m <sup>-3</sup>	Surface density
$g$	—	9.8 m s <sup>-2</sup>	Gravitational acceleration
$c_p$	—	1006 J kg <sup>-1</sup> K <sup>-1</sup>	Specific heat of dry air
$L_v$	—	2.5 × 10 <sup>6</sup> J kg <sup>-1</sup>	Latent heat of vaporization
$R_d$	—	287 J kg <sup>-1</sup> K <sup>-1</sup>	Gas constant for dry air
$R_v$	—	462 J kg <sup>-1</sup> K <sup>-1</sup>	Gas constant for water vapor
$\bar{\epsilon}$	$(R_v/R_d) - 1$	0.61	Coefficient of water vapor for buoyancy
$p_{\text{ref}}$	$\rho_0 u_{\text{ref}}^2$	13 Pa	Reference pressure scale
$\theta_{\text{ref}}$	$\theta_0 u_{\text{ref}}/gt_{\text{ref}}$	3.3 K	Reference potential temperature scale
$q_{\text{ref}}$	$c_p \theta_{\text{ref}}/L_v$	1.3 g kg <sup>-1</sup>	Reference moisture scale
$C_{\text{ref}}$	$c_p \theta_{\text{ref}}/L_v t_{\text{ref}}$	1.3 g kg <sup>-1</sup> (30 s) <sup>-1</sup>	Reference condensation rate
$\Gamma_{\text{ref}}^\theta$	$\theta_{\text{ref}}/t_{\text{ref}}$	3.3 K (30 s) <sup>-1</sup>	Reference heating rate
$\Gamma_{\text{ref}}^q$	—	3.3 K (1 km) <sup>-1</sup>	Reference potential temperature stratification
$B_*$	$c_p \theta_0/L_v$	0.12	Coefficient of moisture for buoyancy
$\Gamma_*^\theta$	$\Gamma_{\text{ref}}^\theta x_{\text{ref}}/\theta_{\text{ref}}$	0.1	Coefficient of background $\theta$ stratification
$\Gamma_*^q$	$\Gamma_{\text{ref}}^q x_{\text{ref}}/q_{\text{ref}}$	0.1	Coefficient of background $q_v$ stratification

$$\begin{aligned}
 \frac{D\mathbf{u}}{Dt} &= -\nabla p + \mathbf{k}\theta + \epsilon \mathbf{k}(\bar{\epsilon}q_v - q_c), \\
 \frac{D\theta}{Dt} + \epsilon \Gamma^\theta w &= C, \\
 \frac{Dq_v}{Dt} + \epsilon \Gamma^q w &= -C, \\
 \frac{Dq_c}{Dt} &= C, \quad \text{and} \\
 \nabla \cdot \mathbf{u} &= 0.
 \end{aligned} \tag{3}$$

Notice that the background stratification terms above are  $O(\epsilon)$  for the assumed stratifications from (2). The three instances of  $\epsilon$  above actually represent three different nondimensional numbers:  $B_* = c_p \theta_0/L_v = q_{\text{ref}} g t_{\text{ref}} u_{\text{ref}}$  is the coefficient of  $\bar{\epsilon}q_v - q_c$  in the buoyancy term;  $\Gamma_*^\theta = \Gamma_{\text{ref}}^\theta x_{\text{ref}}/\theta_{\text{ref}}$  is the coefficient of the background potential temperature stratification; and  $\Gamma_*^q = \Gamma_{\text{ref}}^q x_{\text{ref}}/q_{\text{ref}}$  is the coefficient of the background water vapor stratification. For the reference scales used here, their numerical values are  $B_* = 0.12$ ,  $\Gamma_*^\theta = 0.1$ , and  $\Gamma_*^q = 0.1$ . For the asymptotic expansions below, we thus define the small parameter  $\epsilon = B_* \approx 0.1$ , and we assume that  $\Gamma_*^\theta$  and  $\Gamma_*^q$  are related to  $\epsilon$  in a distinguished limit with  $\Gamma_*^\theta = O(\epsilon)$  and  $\Gamma_*^q = O(\epsilon)$  as  $\epsilon \rightarrow 0$ .

Throughout this paper the focus is on multiscale asymptotic solutions of (3), including both multiple

spatial scales and multiple time scales. Here we introduce some additional scales, besides the parcel scales from above, to illustrate some basic principles of multiscale asymptotics (Kevorkian and Cole 1996). As an example, consider a case with interactions between parcels on scales of  $x_{\text{ref}} = 100$  m,  $t_{\text{ref}} = 30$  s and larger-scale updrafts on scales of  $X_{\text{ref}} = 1000$  m,  $T_{\text{ref}} = 300$  s, which requires larger-scale variables  $\mathbf{X} = (X, Y, Z)$  and  $T$  defined as

$$\mathbf{X} = \epsilon \mathbf{x} \quad \text{and} \quad T = \epsilon t.$$

The two length scales  $\mathbf{x}$  and  $\mathbf{X}$  are then treated as independent variables in some ways. For instance, a general function can depend on  $\mathbf{x}$  and  $\mathbf{X}$  independently in the form  $f(\mathbf{x}, \mathbf{X}, t, T)$ , and the spatial and temporal derivatives are computed using the chain rule as

$$\epsilon \nabla_{\mathbf{X}} + \nabla_{\mathbf{x}} \quad \text{and} \quad \epsilon \partial_T + \partial_t,$$

where  $\nabla_{\mathbf{X}} = (\partial_X, \partial_Y, \partial_Z)$  and  $\nabla_{\mathbf{x}} = (\partial_x, \partial_y, \partial_z)$ .

Means and fluctuations are defined by averaging over the smaller scales. For instance, for a general function  $f(\mathbf{x}, \mathbf{X}, t, T)$ , the integral over the short length scale  $\mathbf{x}$  is used to define the spatial mean and fluctuation:

$$\bar{f}(\mathbf{X}, t, T) = \lim_{L \rightarrow \infty} \frac{1}{(2L)^3} \int_{-L}^L \int_{-L}^L \int_{-L}^L f(\mathbf{x}, \mathbf{X}, t, T) dx dy dz \quad \text{and} \quad f'(\mathbf{x}, \mathbf{X}, t, T) = f - \bar{f}. \tag{4}$$

Notice that the mean  $\bar{f}(\mathbf{X}, t, T)$  depends only on the larger-scale variable  $\mathbf{X}$ , from which it follows that  $\nabla_{\mathbf{x}} \bar{f} = 0$ . These definitions give a separation of any function into its spatial mean and fluctuation as  $f = \bar{f} + f'$ , where, because the scales  $\mathbf{x}$  and  $\mathbf{X}$  are asymptotically separated,  $\bar{f}' = 0$ . Multiple time scales are handled in a similar way, with temporal means and fluctuations defined as

$$\langle f \rangle(\mathbf{x}, \mathbf{X}, T) = \lim_{\sigma \rightarrow \infty} \frac{1}{2\sigma} \int_{-\sigma}^{\sigma} f(\mathbf{x}, \mathbf{X}, t, T) dt \quad \text{and}$$

$$\tilde{f}(\mathbf{x}, \mathbf{X}, t, T) = f - \langle f \rangle. \tag{5}$$

A combined spatial and temporal decomposition can be then be defined as

$$f(\mathbf{x}, \mathbf{X}, t, T) = \langle \bar{f} \rangle(\mathbf{X}, T) + \tilde{\bar{f}}(\mathbf{X}, t, T) + f'(\mathbf{x}, \mathbf{X}, t, T), \tag{6}$$

which follows from expanding  $\bar{f} = \langle \bar{f} \rangle + \tilde{\bar{f}}$  in  $f = \bar{f} + f'$ . A summary of the notation for averages and fluctuations is given in Table 2.

Another important aspect of the method of multiple scale asymptotics is the sublinear growth condition (Kevorkian and Cole 1996; Majda 2003; Majda and Klein 2003). For an informal discussion of this condition, consider an asymptotic expansion of the form

$$f_{\epsilon} = f(t, \epsilon) = f_0(t, \epsilon t) + \epsilon f_1(t, \epsilon t) + \epsilon^2 f_2 + O(\epsilon^3).$$

For this expansion to be useful, the order of magnitude of each term should be as designated; that is, we should have  $f_0 = O(1)$ ,  $\epsilon f_1 = O(\epsilon)$ , and so on, which means that we should have  $f_n = O(1)$  for each  $n$ . Furthermore, we would like this expansion to remain valid on both time scales, that is, for time scales where  $t = O(1)$  and also for the long time scale where  $T = \epsilon t = O(1)$  or, equivalently,  $t = O(\epsilon^{-1})$ . These requirements restrict the way that  $f_n(t, T)$  can depend on  $t$ ; if  $f_n(t, T) = t$ , then  $f_n = \epsilon^{-1}$  when  $t = \epsilon^{-1}$ , which violates the requirement that  $f_n = O(1)$  on the long time scale. To prevent this, we require that  $f_n(t, T)$  grow more slowly than  $t$  as a function of  $t$  (i.e., sublinearly as a function of  $t$ ). For application in a dynamical setting, suppose the short time evolution of  $f_n(t, T)$  is given by

$$\partial_t f_n(t, T) = g(T), \tag{7}$$

where  $g(T)$  is a given  $O(1)$  function that is independent of  $t$ . Since the solution of this equation is  $f_n(t, T) = tg(T) + \text{constant}$ ,  $f_n$  will grow sublinearly as a function of  $t$  if and only if

$$g(T) = 0. \tag{8}$$

TABLE 2. Notation for averages and fluctuations for the case with space scales  $\mathbf{x}$  and  $\mathbf{X} = \epsilon \mathbf{x}$  and time scales  $t$  and  $T = \epsilon t$ .

Notation	Description
$f(\mathbf{x}, \mathbf{X}, t, T)$	A general function of multiple scales
$\bar{f}(\mathbf{X}, t, T)$	Space average of $f$
$f'(\mathbf{x}, \mathbf{X}, t, T)$	Space fluctuation of $f$
$\langle f \rangle(\mathbf{x}, \mathbf{X}, T)$	Time average of $f$
$\tilde{f}(\mathbf{x}, \mathbf{X}, t, T)$	Time fluctuation of $f$
$\langle \bar{f} \rangle(\mathbf{X}, T)$	Space and time average of $f$
$\tilde{\bar{f}}(\mathbf{X}, t, T)$	Space average, time fluctuation of $f$

For a more general case that also appears in this paper, suppose the short time evolution of  $f_n(t, T)$  is given by

$$\partial_t f_n(t, T) = h(t, T), \tag{9}$$

where  $h(t, T)$  is a given  $O(1)$  function that can depend on both  $t$  and  $T$ . In this case,  $f_n(t, T)$  will grow sublinearly as a function of  $t$  if and only if the time average of  $h$  is zero:

$$\langle h \rangle = 0. \tag{10}$$

Physically, this means that a time-mean forcing would lead to linear-in-time growth, where a special case is the  $t$ -independent forcing in (7). A similar discussion applies for the spatial variable  $\mathbf{x}$ , and, for the practical purposes of this paper, a compact way of expressing these sub-linear growth conditions is to say that

$$\overline{\nabla_{\mathbf{x}} f_n} = 0 \quad \text{and} \quad \langle \partial_t f_n \rangle = 0. \tag{11}$$

These conditions will be used often in the derivations below.

### 3. Shallow cumulus: Parcel and updraft scales

Using the scaling for shallow cumulus from the previous section, we can now explore the dynamics implied by this scaling. For example, given typical scaling for cumulus updrafts, is there a simplified dynamics that describes them? And what are the dominant interactions between updrafts and parcels? Using the technique of multiple scale asymptotics from section 2, we now present a multiscale model for shallow cumulus parcels and updrafts, which are shown schematically in Figs. 1 and 2. First, in section 3a, the model is presented; then, in section 3b, the properties of the dynamics are discussed in detail; finally, in section 3c, the model derivation is given.

#### a. The model

For interactions between parcels and updrafts in shallow cumulus, the relevant scales range from  $x_{\text{ref}} = 100 \text{ m}$

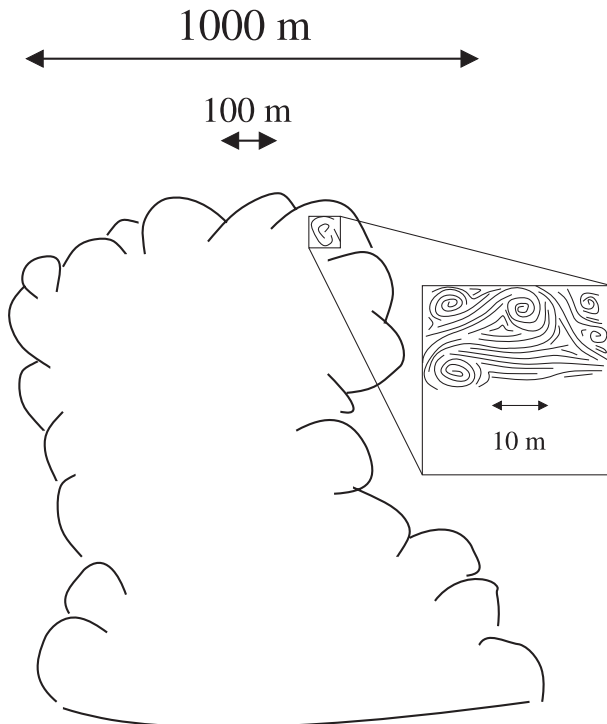


FIG. 1. A schematic diagram of the spatial scales of the shallow cumulus models. The vertical spatial scale is the same as the horizontal spatial scale in each case.

and  $t_{\text{ref}} = 30 \text{ s}$  for parcels to  $X_{\text{ref}} = 1000 \text{ m}$  and  $T_{\text{ref}} = 300 \text{ s}$  for the updraft envelope. Therefore, in addition to the variables  $\mathbf{x}$  and  $t$ , this requires the larger-scale variables defined as

$$\mathbf{X} = \epsilon \mathbf{x} \quad \text{and} \quad T = \epsilon t,$$

where  $\mathbf{X} = (X, Y, Z)$ . Space and time averages are then defined as in (4), (5), and (6), and a summary of notation for averages and fluctuations is given in Table 2.

The multiscale model is obtained by seeking asymptotic solutions to (3) with the form

$$\begin{aligned} \mathbf{u}_\epsilon &= \bar{\mathbf{U}}(\epsilon \mathbf{x}, t, \epsilon t) + \mathbf{U}'(\mathbf{x}, \epsilon \mathbf{x}, t, \epsilon t) + \epsilon \mathbf{u} + O(\epsilon^2), \\ \theta_\epsilon &= \bar{\Theta}(\epsilon \mathbf{x}, t, \epsilon t) + \Theta'(\mathbf{x}, \epsilon \mathbf{x}, t, \epsilon t) + \epsilon \theta + O(\epsilon^2), \\ q_{v,\epsilon} &= \bar{Q}_v(\epsilon \mathbf{x}, t, \epsilon t) + Q'_v(\mathbf{x}, \epsilon \mathbf{x}, t, \epsilon t) + \epsilon q_v + O(\epsilon^2), \\ q_{c,\epsilon} &= \bar{Q}_c(\epsilon \mathbf{x}, t, \epsilon t) + Q'_c(\mathbf{x}, \epsilon \mathbf{x}, t, \epsilon t) + \epsilon q_c + O(\epsilon^2), \\ p_\epsilon &= \epsilon^{-1} \bar{P}_{-1}(\epsilon \mathbf{x}, t, \epsilon t) + \bar{P}(\epsilon \mathbf{x}, t, \epsilon t) + P'(\mathbf{x}, \epsilon \mathbf{x}, t, \epsilon t) \\ &\quad + \epsilon p + O(\epsilon^2), \quad \text{and} \\ C_\epsilon &= \bar{C}(\epsilon \mathbf{x}, t, \epsilon t) + C'(\mathbf{x}, \epsilon \mathbf{x}, t, \epsilon t) + \epsilon c + O(\epsilon^2), \end{aligned} \tag{12}$$

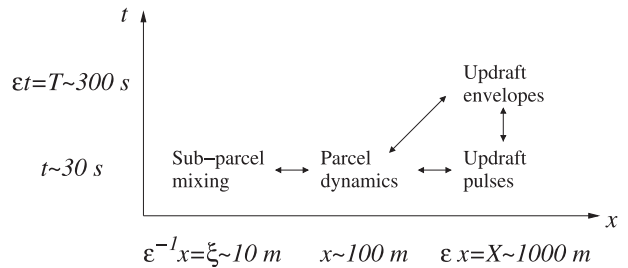


FIG. 2. The shallow cumulus models and their spatial and temporal scales. The vertical spatial scale is the same as the horizontal spatial scale in each case.

where the subscript  $\epsilon$  denotes that  $q_{v,\epsilon}(\mathbf{x}, t)$  is a function of  $\mathbf{x}$  and  $t$  and the parameter  $\epsilon$ . The model consists of dynamics on the three scales shown in the decomposition in (6): parcels  $Q'_v$ , updraft pulses  $\bar{Q}_v$ , and updraft envelopes  $\langle \bar{Q}_v \rangle$ . The dynamics and interactions of these three scales of motion are given by the following three equation sets, which we identify by names as follows: *nonlinear parcel dynamics*,

$$\begin{aligned} \frac{D'}{Dt} \mathbf{U}' &= -\nabla' P' + \mathbf{k} \Theta', \\ \frac{D'}{Dt} \Theta' &= C', \\ \frac{D'}{Dt} Q'_v &= -C', \\ \frac{D'}{Dt} Q'_c &= C', \quad \text{and} \\ \nabla' \cdot \mathbf{U}' &= 0, \end{aligned} \tag{13}$$

where  $\nabla' = (\partial_x, \partial_y, \partial_z)$  and

$$\frac{D'}{Dt} = \partial_t + (\langle \bar{\mathbf{U}} \rangle + \tilde{\mathbf{U}} + \mathbf{U}') \cdot \nabla';$$

*linear updraft pulses*,

$$\begin{aligned} \partial_t \tilde{\mathbf{U}} &= -\bar{\nabla} \tilde{P}_{-1} + \mathbf{k} \tilde{\Theta}, \\ \partial_t \tilde{\Theta} &= \tilde{C}, \\ \partial_t \tilde{Q}_v &= -\tilde{C}, \\ \partial_t \tilde{Q}_c &= \tilde{C}, \quad \text{and} \\ \bar{\nabla} \cdot \tilde{\mathbf{U}} &= 0, \end{aligned} \tag{14}$$

where  $\bar{\nabla} = (\partial_X, \partial_Y, \partial_Z)$ ; and *balanced updraft envelopes*,

$$\begin{aligned}
 \langle \bar{C} \rangle &= 0, \\
 \langle \bar{\theta} \rangle &= 0, \\
 \frac{\bar{D}}{DT} \langle \bar{\mathbf{U}}_h \rangle &= -\bar{\nabla}_h \langle \bar{P} \rangle - \bar{\nabla} \cdot \langle \bar{\mathbf{U}}' : \bar{\mathbf{U}}'_h \rangle - \bar{\nabla} \cdot \langle \tilde{\mathbf{U}} : \tilde{\mathbf{U}}_h \rangle, \\
 \langle \bar{\theta} \rangle &= -\frac{\bar{D}}{DT} \langle \bar{W} \rangle - \partial_Z \langle \bar{P} \rangle + \bar{\epsilon} \langle \bar{Q}_v \rangle - \langle \bar{Q}_c \rangle \\
 &\quad - \bar{\nabla} \cdot \langle \bar{\mathbf{U}}' \bar{W}' \rangle - \bar{\nabla} \cdot \langle \tilde{\mathbf{U}} \tilde{W} \rangle, \\
 \Gamma^\theta \langle \bar{W} \rangle &= \langle \bar{c} \rangle - \bar{\nabla} \cdot \langle \bar{\mathbf{U}}' \bar{\theta}' \rangle - \bar{\nabla} \cdot \langle \tilde{\mathbf{U}} \tilde{\theta} \rangle, \\
 \frac{\bar{D}}{DT} \langle \bar{Q}_v \rangle + \Gamma^q \langle \bar{W} \rangle &= -\langle \bar{c} \rangle - \bar{\nabla} \cdot \langle \bar{\mathbf{U}}' \bar{Q}'_v \rangle - \bar{\nabla} \cdot \langle \tilde{\mathbf{U}} \tilde{Q}_v \rangle, \\
 \frac{\bar{D}}{DT} \langle \bar{Q}_c \rangle &= \langle \bar{c} \rangle - \bar{\nabla} \cdot \langle \bar{\mathbf{U}}' \bar{Q}'_c \rangle - \bar{\nabla} \cdot \langle \tilde{\mathbf{U}} \tilde{Q}_c \rangle, \quad \text{and} \\
 \bar{\nabla}_h \cdot \langle \bar{\mathbf{U}}_h \rangle &= -\partial_Z \langle \bar{W} \rangle,
 \end{aligned} \tag{15}$$

where

$$\frac{\bar{D}}{DT} = \partial_T + \langle \bar{\mathbf{U}} \rangle \cdot \bar{\nabla}$$

and where  $\mathbf{U}_h = (U, V, 0)$  is the horizontal velocity,  $\bar{\nabla}_h = (\partial_X, \partial_Y, 0)$  is the horizontal gradient, and the colon has the meaning  $(\mathbf{U} : \mathbf{U}_h)_i = \mathbf{U} \mathbf{U}_{h,i}$  for  $i = 1, 2$ .

*b. Discussion*

The model (13)–(15) describes interactions between three paradigms of cumulus convection: parcels, pulses, and updrafts. To gain further insight, the model is discussed here in two contexts: 1) properties of the equations and 2) phenomena of shallow cumulus dynamics.

1) PROPERTIES OF THE EQUATIONS

The model in (13)–(15) encompasses three different types of dynamics on the three different scales of the decomposition in (6). On the smallest scales are the parcel dynamics of  $Q'_v(\mathbf{x}, \mathbf{X}, t, T)$  in (13); this dynamics involves both spatial and temporal fluctuations as functions of both  $\mathbf{x}$  and  $t$  with  $\mathbf{X}$  and  $T$  treated as frozen parameters. On the same fast time scale  $t$  but larger spatial scales  $\mathbf{X}$  are the updraft pulses  $\tilde{Q}_v(\mathbf{X}, t, T)$  in (14), where  $T$  is treated as a frozen parameter. Finally, on the slow time scale  $T$  and large spatial scales  $\mathbf{X}$  are the balanced updraft envelopes  $\langle \bar{Q}_v \rangle(\mathbf{X}, T)$  in (15). Next, each of these three dynamics is discussed in this order.

On the short 100-m length scales and fast time scale  $t$  in (13) are the parcel dynamics of  $Q'_v$ . These equations are essentially the nonlinear, unstratified Boussinesq equations where the buoyancy at leading order does not include moisture contributions. The parcel dynamics are

not isolated, however; the updraft pulses and updraft envelope affect the parcels through advection by  $\bar{\mathbf{U}}$  and  $\langle \bar{\mathbf{U}} \rangle$ , respectively. One might also expect that large-scale shear terms of the form  $\mathbf{U}' \cdot \bar{\nabla} \tilde{Q}_v$  could potentially generate turbulence on the  $O(100 \text{ m})$  parcel scales; however, these terms appear here at  $O(\epsilon)$  and are therefore not part of the leading-order dynamics of (13). There is, however, another way that the updrafts affect the parcels: the condensation term  $C'(\mathbf{x}, \mathbf{X}, t, T)$  is a nonlinear function of the thermodynamic state, which is determined at leading order by the sum of contributions from each scale such as  $\langle \bar{Q}_v \rangle(\mathbf{X}, T) + \tilde{Q}_v(\mathbf{X}, t, T) + Q'_v(\mathbf{x}, \mathbf{X}, t, T)$ . In other words, the larger-scale fields such as  $\langle \bar{Q}_v \rangle(\mathbf{X}, T)$  and  $\tilde{Q}_v(\mathbf{X}, t, T)$  provide a thermodynamic background state for the parcels because

$$[f(Q'_v)]' \neq f(Q'_v) \text{ for a nonlinear function } f; \tag{16}$$

that is,  $[f(Q'_v)]'$  depends not only on  $Q'_v$  but also on  $\tilde{Q}_v$  and  $\langle \bar{Q}_v \rangle$  for a nonlinear function  $f$  such as the condensation.

On the same fast time scale  $t$  but on the larger 1000-m spatial scales are the updraft pulses  $\tilde{Q}_v$  in (14). On these scales, advection terms are absent (i.e., the dynamical core is linear), and the other scales are felt here only through the nonlinear condensation  $\bar{C}(\mathbf{X}, t, T)$ . The condensation on these scales is the spatial average of the condensation over the smaller 100-m parcel scales, and it is a function of not only the updraft pulse variables such as  $\tilde{Q}_v$  but also the parcel fluctuations  $Q'_v$  and updraft envelopes  $\langle \bar{Q}_v \rangle$ ; this is because

$$\bar{f}(\bar{Q}_v) \neq f(\bar{Q}_v) \text{ for a nonlinear function } f. \tag{17}$$

Finally, on the 1000-m spatial scales and slow time scale  $T$  are the balanced updraft envelopes  $\langle \bar{Q}_v \rangle$  in (15). These dynamics are balanced in the sense that the leading-order potential temperature  $\langle \bar{\theta} \rangle$  and vertical velocity  $\langle \bar{W} \rangle$  are given by diagnostic balance conditions, while the other variables evolve prognostically. This is a shallow cumulus-scale version of the so-called weak-temperature-gradient models that have been developed previously for larger-scale tropical dynamics (Sobel et al. 2001; Majda and Klein 2003; Majda et al. 2008). The balance condition for  $\langle \bar{W} \rangle$  comes from the potential temperature equation and represents balance between ascent/descent and heat sources, which include condensation  $\langle \bar{c} \rangle$  and eddy fluxes  $\bar{\nabla} \cdot \langle \bar{\mathbf{U}}' \bar{Q}'_v \rangle$  and  $\bar{\nabla} \cdot \langle \tilde{\mathbf{U}} \tilde{Q}_v \rangle$  from the parcels and updraft pulses, respectively. The eddy fluxes can be thought of as subadiabatic terms in this context, and the averaged heating  $\langle \bar{c} \rangle(\mathbf{X}, T)$  is a function of not only the updraft envelope fields such as  $\langle \bar{Q}_v \rangle$  but also the fluctuations; this latter effect is due to the nonlinear nature of the condensation rate as explained in (17).

Also notice that the parcel-scale condensation/evaporation fluctuations  $C'(\mathbf{x}, \mathbf{X}, t, T)$  are allowed to be larger than the condensation/evaporation  $\epsilon(\bar{c})(\mathbf{X}, T)$  on the updraft envelope scales; that is,  $C'$  is allowed to be as large as  $O[1.3 \text{ g kg}^{-1} (30 \text{ s})^{-1}]$ , whereas  $\epsilon(\bar{c}) = O[1.3 \text{ g kg}^{-1} (300 \text{ s})^{-1}]$ . While a major contributor to  $\epsilon(\bar{c})$  is adiabatic compression/expansion, as represented in (15) by the effect of  $\Gamma^q \langle \bar{W} \rangle$ , this is not a leading-order effect on parcel scales, as reflected by the absence of a parcel-scale term  $\Gamma^q W'$  in (13). This is because adiabatic compression/expansion is only felt at leading order on the longer  $T$  time scale, after a parcel has ascended/descended an appreciable vertical distance of  $O(1000 \text{ m})$ . Parcel-scale fluctuations  $C'$  of  $O[1.3 \text{ g kg}^{-1} (30 \text{ s})^{-1}]$  could arise from another mechanism: mixing of cloudy and cloud-free air. On the parcel time scale of  $O(30 \text{ s})$ , for the mixing of cloud-free air and cloudy air with an  $O(1.3 \text{ g kg}^{-1})$  cloud condensate anomaly, an evaporation anomaly  $C'$  of  $O[1.3 \text{ g kg}^{-1} (30 \text{ s})^{-1}]$  could be produced. The averaged effect of this parcel-scale mixing then contributes to  $\epsilon(\bar{c})$  at  $O[1.3 \text{ g kg}^{-1} (300 \text{ s})^{-1}]$  on the updraft envelope scales, at the same order of magnitude as the effect of adiabatic compression/expansion.

To summarize the dynamical aspects of the multiscale interactions, two of the main features are that (i) updraft envelopes obey a balanced dynamics in the form of a cloud-scale weak-temperature-gradient model and (ii) parcels affect updrafts through upscale eddy flux terms such as  $\bar{\mathbf{V}} \cdot \langle \mathbf{U}' \mathbf{Q}'_v \rangle$  but updrafts do not affect parcels through large-scale gradients such as  $\mathbf{U}' \cdot \bar{\nabla} \mathbf{Q}_v$ . In the sense of this latter point, the multiscale model suggests that *shallow cumulus dynamics are parcel dominated* rather than updraft dominated.

## 2) PHENOMENOLOGY OF SHALLOW CUMULUS DYNAMICS

In terms of shallow cumulus phenomena, one can see that these three types of dynamics in (13)–(15) describe three paradigms of shallow cumulus dynamics that are seen in observations and simulations: parcels, pulses, and updrafts. First, the notion of cloud parcels is well known and pervasive (Rogers and Yau 1989; Houze 1993), and the various aspects of their dynamics are included in (13): ascent/descent driven by condensation and buoyancy, and nonlinear advection, transport, and deformation, among others. Second, the dynamics in (14) have been called “updraft pulses” here because of their similarity to the “pulses” seen in observations (French et al. 1999) and in simulations (Carpenter et al. 1998a; Zhao and Austin 2005; Heus et al. 2009). In the model here, the pulses are  $O(1000 \text{ m})$  envelopes of parcels and are driven by the averaged heating over the envelope; they advect the smaller-scale parcels, and they

appear as temporal fluctuations to the balanced updraft. In the simulations of Heus et al. (2009), the pulses have spatial scales of  $O(1000 \text{ m})$ , and several pulses typically occur within the lifetime of a cloud. These similarities suggest that the dynamics in (14) correspond to the observed and simulated updraft pulses. Third, and finally, the dynamics in (15) represent the balanced dynamics of a cloud updraft over its lifetime, averaged over all the fluctuations due to parcels and pulses. This balanced updraft is driven by averaged heating and eddy fluxes from the parcels and pulses; in turn, it advects the smaller-scale parcels and provides a background thermodynamic state for them.

With an understanding of these processes at hand, it is seen that these three paradigms and their relevant scales are consistent with, and can be used to rationalize, the results of numerical simulations. For instance, in order to resolve the  $O(100 \text{ m})$  parcel dynamics in (13), a grid spacing of  $O(10 \text{ m})$  would be required. Examples of this include Brown (1999), Stevens et al. (2001), and Stevens et al. (2002), which clearly show finescale structures within updrafts when  $\Delta x = O(10 \text{ m})$  rather than  $\Delta x = O(100 \text{ m})$ . If a coarse grid spacing of  $O(100 \text{ m})$  is used, then one would expect the updraft pulses (14) and updraft envelopes (15) to be resolved faithfully; ideally, the effect of the  $O(100 \text{ m})$  parcels is represented by subgrid-scale parameterization. One example of this is the simulations of Stevens and Seifert (2008), in which a cloud lifetime consists of a single updraft pulse, and the  $O(100 \text{ m})$  parcels are only marginally resolved.

### c. Derivation

The derivation of the parcel/updraft model in (13)–(15) is as follows. Upon inserting the ansatz (12) into (3), the  $O(1)$  part of the continuity equation is  $\nabla' \cdot \mathbf{U}' = 0$ , which is the continuity equation in (13) for the parcel dynamics. The  $O(\epsilon)$  part of the continuity equation is  $\bar{\nabla} \cdot \bar{\mathbf{U}} + \bar{\nabla} \cdot \mathbf{U}' + \nabla' \cdot \mathbf{u}' = 0$ . Using the condition in (11), the spatial mean of this is  $\bar{\nabla} \cdot \bar{\mathbf{U}} = 0$ . The time mean and fluctuation of this equation are then the continuity equations in (15) and (14), respectively.

For the derivation of the evolution equations on the short time scale  $t$ , (13) and (14), we first consider the potential temperature. To proceed, insert the ansatz (12) into (3) and collect the  $O(1)$  terms:

$$\partial_t \Theta + \nabla' \cdot (\mathbf{U} \Theta) = C,$$

where  $\nabla' \cdot \mathbf{U} = 0$  was used to write the advection terms in conservative form. This equation can be split into its spatial mean and fluctuation by using the condition in (11), which leads to (13) for the spatial fluctuation and

$$\partial_t \bar{\Theta} = \bar{C}$$

for the spatial mean. Recall from section 2 that  $\bar{\Theta}$  must have sublinear growth as a function of  $t$  in order for the asymptotic ordering in (12) to remain valid. Since the equation above is of the form (9), the variable  $\bar{\Theta}$  will grow sublinearly as a function of  $t$  if and only if

$$\langle \bar{C} \rangle = 0.$$

Physically, this condition takes the following meaning: if  $\langle \bar{C} \rangle$  were nonzero, then  $\bar{\Theta}$  could potentially grow as large as  $O(30 \text{ K})$ . This provides the derivation for this condition in the balanced updraft model in (15). It also leads to the potential temperature evolution for updraft pulses in (14) after also noting that  $\partial_t f = \partial_t \tilde{f}$  for any general function  $f(t, T) = \langle f \rangle(T) + \tilde{f}(t, T)$ . Note that the condition  $\langle \bar{\Theta} \rangle = 0$  arises independently but for a similar reason, as explained in the next paragraph.

For the derivation of the velocity equations, the  $O(1)$  terms are

$$\partial_t \mathbf{U} + \mathbf{V}' \cdot (\mathbf{U} : \mathbf{U}) = -\bar{\mathbf{V}} \tilde{P}'_{-1} - \mathbf{V}' P' + \mathbf{k} \Theta,$$

where the colon has the meaning  $(\mathbf{U} : \mathbf{U})_i = \mathbf{U} U_i$  for  $i = 1, 2, 3$ . This equation can be split into its spatial mean and fluctuation by using the condition in (11), which leads to (13) for the spatial fluctuation and to

$$\partial_t \tilde{\mathbf{U}} + \bar{\mathbf{V}} \tilde{P}'_{-1} = \mathbf{k} \bar{\Theta}, \quad \bar{\mathbf{V}} \cdot \tilde{\mathbf{U}} = 0$$

for the spatial mean, where the continuity equation has also been listed here. As was the case for the potential temperature above, it must be ensured that  $\tilde{\mathbf{U}}$  and  $\tilde{P}'_{-1}$  grow sublinearly as functions of  $t$  in order for the asymptotic ordering in (12) to remain valid. For the linear system of equations above for  $\tilde{\mathbf{U}}$  and  $\tilde{P}'_{-1}$ , sublinear growth of  $\tilde{\mathbf{U}}$  and  $\tilde{P}'_{-1}$  occurs if and only if

$$\langle \bar{\Theta} \rangle = 0, \tag{18}$$

which is explained in more detail at the end of this section for a more general situation. Physically, this condition takes the following meaning: if  $\langle \bar{\Theta} \rangle$  were nonzero, then  $\tilde{\mathbf{U}}$  could potentially grow as large as  $O(33 \text{ m s}^{-1})$ . This provides the derivation for this condition in the balanced updraft dynamics in (15), and it also leads to the velocity equations in the updraft pulse model (14).

To arrive at the evolution equations on longer times, the ansatz (12) is inserted into (3) and the  $O(\epsilon)$  terms are collected; then a spatial average is applied to give the potential temperature equation

$$\partial_t \bar{\theta} = -\partial_T \bar{\Theta} - \bar{\mathbf{V}} \cdot (\bar{\mathbf{U}} \bar{\Theta}) - \Gamma^\theta \bar{W} + \bar{c}. \tag{19}$$

Note that this is an equation of the form  $\partial_t \bar{\theta} = \bar{h}(t, T)$  where  $T$  is treated as a frozen parameter. Therefore,  $\bar{\theta}$

grows sublinearly as a function of  $t$  if and only if  $\langle \bar{h} \rangle = 0$ ; that is,

$$\bar{\mathbf{V}} \cdot \langle \bar{\mathbf{U}} \bar{\Theta} \rangle + \Gamma^\theta \langle \bar{W} \rangle = \langle \bar{c} \rangle,$$

where it was also used that  $\langle \bar{\Theta} \rangle = 0$  from (18). This is the diagnostic relationship that determines  $\langle \bar{W} \rangle$  in (15), where the eddy flux term is split into means and fluctuations as

$$\begin{aligned} \langle \bar{\mathbf{U}} \bar{\Theta} \rangle &= \langle \bar{\mathbf{U}} \bar{\Theta} \rangle + \langle \bar{\mathbf{U}}' \bar{\Theta}' \rangle \\ &= \langle \bar{\mathbf{U}} \rangle \langle \bar{\Theta} \rangle + \langle \tilde{\mathbf{U}} \tilde{\Theta} \rangle + \langle \bar{\mathbf{U}}' \bar{\Theta}' \rangle \\ &= 0 + \langle \tilde{\mathbf{U}} \tilde{\Theta} \rangle + \langle \bar{\mathbf{U}}' \bar{\Theta}' \rangle. \end{aligned}$$

To obtain the velocity equations on longer times, proceed as was done for (19) to arrive at

$$\begin{aligned} \partial_t \tilde{\mathbf{u}} + \bar{\mathbf{V}} \tilde{P}' &= -\partial_T \bar{\mathbf{U}} - \bar{\mathbf{V}} \cdot (\bar{\mathbf{U}} : \bar{\mathbf{U}}) - \bar{\mathbf{V}} \langle \bar{P} \rangle + \mathbf{k} \bar{\theta} + \mathbf{k} (\bar{\epsilon} \bar{Q}_v - \bar{Q}_c) \\ &= \bar{\mathbf{h}}(\mathbf{X}, t, T), \\ \bar{\mathbf{V}} \cdot \tilde{\mathbf{u}} &= 0, \end{aligned} \tag{20}$$

where the incompressibility condition arises from (3) at  $O(\epsilon^2)$  after taking a spatial mean. This is a linear system of partial differential equations for the vector  $\tilde{\mathbf{u}}$  and the pressure  $\tilde{P}'$  as functions of  $\mathbf{X}$  and  $t$ , where  $T$  is treated as a frozen parameter and where the source term  $\bar{\mathbf{h}}$  on the right-hand side depends on  $\mathbf{X}$ ,  $t$ , and  $T$ .

We must ensure sublinear growth of  $\tilde{\mathbf{u}}$  and  $\tilde{P}'$  as functions of  $t$ . To accomplish this, apply a curl and divergence to (20) to obtain, respectively,

$$\partial_t \tilde{\omega} = \bar{\mathbf{V}} \times \bar{\mathbf{h}} \quad \text{and} \quad -\bar{\mathbf{V}}^2 \tilde{P}' = \bar{\mathbf{V}} \cdot \bar{\mathbf{h}},$$

where  $\tilde{\omega} = \bar{\mathbf{V}} \times \tilde{\mathbf{u}}$ . Now the same sublinear growth condition of (9) can be applied to each component of  $\tilde{\omega}$  to arrive at  $\bar{\mathbf{V}} \times \langle \bar{\mathbf{h}} \rangle = 0$ ; and applying a time average to the second equation leads to the condition  $\bar{\mathbf{V}} \cdot \langle \bar{\mathbf{h}} \rangle = 0$  in order to ensure that  $\tilde{P}'$  maintains a time mean of zero. The derivation is thus complete since  $\bar{\mathbf{V}} \times \langle \bar{\mathbf{h}} \rangle = 0$  and  $\bar{\mathbf{V}} \cdot \langle \bar{\mathbf{h}} \rangle = 0$  are the vorticity form of the velocity equations in (15).

#### 4. Shallow cumulus: Parcel and subparcel scales

In the previous section, a class of parcel-updraft interactions was described, and it was seen that the interactions are dominated by upscale eddy fluxes. In this section we consider interactions on smaller scales between parcels and subparcel turbulent mixing. What is the nature of these smaller-scale interactions? Are these interactions also dominated by upscale eddy fluxes? Below, a multiscale model is developed for the interaction between parcel and subparcel scales, and it will be

compared and contrasted with the parcel/updraft model of section 3. These different models and scales are summarized schematically in Figs. 1 and 2.

The model in this section is developed to describe interactions between parcels on scales of  $x_{\text{ref}} = 100$  m and subparcel turbulent mixing on scales of  $\xi_{\text{ref}} = 10$  m. In addition to the variables  $\mathbf{x}$  and  $t$ , this requires the smaller-scale variables defined as

$$\boldsymbol{\xi} = \epsilon^{-1} \mathbf{x} \quad \text{and} \quad \tau = \epsilon^{-1} t,$$

where  $\boldsymbol{\xi} = (\xi, \eta, \zeta)$  and  $\tau_{\text{ref}} = 3$  s. Asymptotic solutions to (3) are then developed with the form

$$\begin{aligned} \mathbf{u}_\epsilon &= [\langle \bar{\mathbf{U}} \rangle(\mathbf{x}, t) + \epsilon \bar{\mathbf{u}}(\mathbf{x}, t, \epsilon^{-1} t)] + \epsilon \mathbf{u}'(\mathbf{x}, \epsilon^{-1} \mathbf{x}, t, \epsilon^{-1} t) \\ &\quad + \epsilon^2 \mathbf{u}_2 + O(\epsilon^3), \\ \theta_\epsilon &= [\langle \bar{\Theta} \rangle(\mathbf{x}, t) + \epsilon \bar{\theta}] + \epsilon \theta' + \epsilon^2 \theta_2 + O(\epsilon^3), \\ q_{v,\epsilon} &= [\langle \bar{Q}_v \rangle(\mathbf{x}, t) + \epsilon \bar{q}_v] + \epsilon q'_v + \epsilon^2 q_{v,2} + O(\epsilon^3), \\ q_{c,\epsilon} &= [\langle \bar{Q}_c \rangle(\mathbf{x}, t) + \epsilon \bar{q}_c] + \epsilon q'_c + \epsilon^2 q_{c,2} + O(\epsilon^3), \\ p_\epsilon &= [\langle \bar{P} \rangle(\mathbf{x}, t) + \epsilon \bar{p} + \epsilon^2 \bar{p}_2] + \epsilon^2 p'_2 + \epsilon^3 p_3 + O(\epsilon^4), \quad \text{and} \\ C_\epsilon &= [\langle \bar{C} \rangle(\mathbf{x}, t) + \epsilon \bar{c}] + \epsilon c' + O(\epsilon^2), \end{aligned} \quad (21)$$

where  $\bar{f} = \bar{f}(\mathbf{x}, t, \tau)$  and  $\langle f \rangle = \langle f \rangle(\mathbf{x}, \boldsymbol{\xi}, t)$  now represent spatial and temporal averages over the shorter space and time scales  $\boldsymbol{\xi}$  and  $\tau$ , respectively. The precise definitions of these averages are given in the appendix. Also notice that the weaker variables  $\epsilon \mathbf{u}'$  represent the smaller-scale turbulent fluctuations, and their amplitude of roughly  $0.33 \text{ m s}^{-1} \approx \epsilon u_{\text{ref}}$  is consistent with inertial-range scaling of turbulence in the atmosphere:

$$u_{\text{turb}} \approx (D \xi_{\text{ref}})^{1/3} \approx 0.46 \text{ m s}^{-1}, \quad (22)$$

where  $D = 10^{-2} \text{ m}^2 \text{ s}^{-3}$  is a typical atmospheric energy dissipation rate.

With the ansatz from (21), the parcel/subparcel model is given by the following three sets of equations: *non-linear parcel dynamics*,

$$\begin{aligned} \frac{\bar{D}}{Dt} \bar{\mathbf{U}} &= -\bar{\nabla} \bar{P} + \mathbf{k} \bar{\Theta}, \\ \frac{\bar{D}}{Dt} \bar{\Theta} &= \bar{c}, \\ \frac{\bar{D}}{Dt} \bar{Q}_v &= -\bar{c}, \\ \frac{\bar{D}}{Dt} \bar{Q}_c &= \bar{c}, \quad \text{and} \\ \bar{\nabla} \cdot \bar{\mathbf{U}} &= 0, \end{aligned} \quad (23)$$

where  $\bar{\nabla} = (\partial_x, \partial_y, \partial_z)$  and

$$\frac{\bar{D}}{Dt} = \partial_t + \bar{\mathbf{U}} \cdot \bar{\nabla};$$

*subparcel turbulent mixing*,

$$\begin{aligned} \frac{D'}{Dt} \mathbf{u}' + \mathbf{u}' \cdot \bar{\nabla} \bar{\mathbf{U}} &= -\bar{\nabla}' p'_2 + \mathbf{k} \theta', \\ \frac{D'}{Dt} \theta' + \mathbf{u}' \cdot \bar{\nabla} \bar{\Theta} &= c', \\ \frac{D'}{Dt} q'_v + \mathbf{u}' \cdot \bar{\nabla} \bar{Q}_v &= -c', \\ \frac{D'}{Dt} q'_c + \mathbf{u}' \cdot \bar{\nabla} \bar{Q}_c &= c', \quad \text{and} \\ \bar{\nabla}' \cdot \mathbf{u}' &= 0, \end{aligned} \quad (24)$$

where  $\bar{\nabla}' = (\partial_\xi, \partial_\eta, \partial_\zeta)$  and

$$\frac{D'}{Dt} = \partial_t + \bar{\mathbf{U}} \cdot \bar{\nabla} + (\bar{\mathbf{u}} + \mathbf{u}') \cdot \bar{\nabla}';$$

and *weaker linear parcel fluctuations*,

$$\begin{aligned} \frac{\bar{D}}{Dt} \bar{\mathbf{u}} + \bar{\mathbf{u}} \cdot \bar{\nabla} \bar{\mathbf{U}} &= -\bar{\nabla} \bar{p} + \mathbf{k}(\bar{\theta} + \bar{c} \bar{Q}_v - \bar{Q}_c), \\ \frac{\bar{D}}{Dt} \bar{\theta} + \bar{\mathbf{u}} \cdot \bar{\nabla} \bar{\Theta} + \Gamma^{\theta} \bar{W} &= \bar{c}, \\ \frac{\bar{D}}{Dt} \bar{q}_v + \bar{\mathbf{u}} \cdot \bar{\nabla} \bar{Q}_v + \Gamma^q \bar{W} &= -\bar{c}, \\ \frac{\bar{D}}{Dt} \bar{q}_c + \bar{\mathbf{u}} \cdot \bar{\nabla} \bar{Q}_c &= \bar{c}, \quad \text{and} \\ \bar{\nabla} \cdot \bar{\mathbf{u}} &= 0, \end{aligned} \quad (25)$$

where all variables in (23)–(25) are time-averaged variables but the angle brackets  $\langle \cdot \rangle$  have been left off to ease notation. The derivation of (23)–(25) and the precise definitions of space and time averages are given in the appendix.

Notice that the nonlinear parcel dynamics on scales of  $O(100 \text{ m})$  are the same here in (23) as they were in (13) if advection by updrafts is ignored in (13). While the dynamics is the same, the notation differs between (13) and (23) because the  $O(100 \text{ m})$  parcels are spatial fluctuations (with primes such as  $Q'_v$ ) in the context of parcel/updraft dynamics and spatial averages (with overbars such as  $\bar{Q}_v$ ) in the context of parcel/subparcel dynamics. The intersection of these models at the  $O(100 \text{ m})$  parcel scales can be seen in the schematic diagrams in Figs. 1 and 2.

In comparison to the parcel/updraft model of section 3, one important difference here is that the spatial fluctuations

TABLE 3. Reference scales for the deep cumulus models. Any reference scales that are the same as those for shallow cumulus in Table 1 are not repeated here.

Parameter	Derivation	Value	Description
$u_{\text{ref}}$	—	10 m s <sup>-1</sup>	Reference velocity scale
$x_{\text{ref}}$	—	1 km	Reference length scale
$t_{\text{ref}}$	$x_{\text{ref}}/u_{\text{ref}}$	100 s	Reference time scale
$p_{\text{ref}}$	$\rho_0 u_{\text{ref}}^2$	120 Pa	Reference pressure scale
$C_{\text{ref}}$	$c_p \theta_{\text{ref}}/L_v f_{\text{ref}}$	1.3 g kg <sup>-1</sup> (100 s) <sup>-1</sup>	Reference condensation rate
	$\theta_{\text{ref}}/t_{\text{ref}}$	3.3 K (100 s) <sup>-1</sup>	Reference heating rate
$\Gamma_{*}^{\theta}$	$\Gamma_{\text{ref}}^{\theta} x_{\text{ref}}/\theta_{\text{ref}}$	1	Coefficient of background $\theta$ stratification
$\Gamma_{*}^q$	$\Gamma_{\text{ref}}^q x_{\text{ref}}/q_{\text{ref}}$	1	Coefficient of background $q_v$ stratification

$q'_v$  are affected by larger-scale gradients through the term  $\mathbf{u}' \cdot \bar{\nabla} \bar{Q}_v$ , but the larger-scale fields are not affected by the eddy fluxes  $\bar{\nabla} \cdot \mathbf{u}' q'_v$  at leading order; the opposite was true for the parcel/updraft model in section 3. This difference is largely due to the different scales involved, as shown in the ansatzes of the two cases in (12) and (21); parcels and updrafts are described by  $O(1)$  fields, whereas subparcel fluctuations are  $O(\epsilon)$  in magnitude and agree with turbulent inertial-range scaling as explained in (22).

Another striking difference from the parcel/updraft model of section 3 is that (23)–(25) involve only a single time scale. In other words, the  $O(100 \text{ m})$  parcels and  $O(10 \text{ m})$  subparcel mixing occur on different spatial scales but share a common time scale. This is consistent with previous work that has shown that entrainment/turbulent mixing occurs on the same time scale as larger-scale cloud dynamics (Baker et al. 1984; Krueger et al. 1997; Grabowski 2007), and the cloud droplet spectrum can be affected by the mixing scenario, depending on whether it is homogeneous mixing, extremely inhomogeneous mixing, or an intermediate scenario (Su et al. 1998; Morrison and Grabowski 2008; Andrejczuk et al. 2009).

Finally, another key difference is the appearance of a new advection term of the form  $\bar{\mathbf{U}} \cdot \bar{\nabla} q'_v$  for the subparcel turbulent fluctuations in (24). Notice that this represents parcel-scale gradients  $\bar{\nabla}$  of the subparcel-scale fluctuations  $q'_v$ . The meaning of this term can be seen in the evolution equation for  $\overline{q_v'^2}$ , which is found from (24) by multiplying by  $q'_v$  and taking a spatial average:

$$\partial_t \overline{q_v'^2} + \bar{\mathbf{U}} \cdot \bar{\nabla} \overline{q_v'^2} = -2\overline{q'_v \mathbf{u}' \cdot \bar{\nabla} \bar{Q}_v} - 2\overline{q'_v c'}. \quad (26)$$

This new advection term therefore represents parcel-scale advection of subparcel-scale variance, as is sometimes used in subgrid-scale closures in large-eddy simulations [see Sommeria (1976) and Stevens et al. (2001) and references therein]. Hence, the scaling used in this section represents a scenario where such advection terms appear at leading order, although their effects on the larger scales

through upscale eddy fluxes are not present at leading order (but may accumulate over longer time scales).

### 5. Deep cumulus

In sections 3 and 4, multiscale models were developed for shallow cumulus. In what ways are deep cumulus dynamics different from shallow cumulus? For instance, are the parcel–updraft interactions for deep cumulus also dominated by upscale eddy fluxes? Below, we develop the deep cumulus analogs of the shallow cumulus models, and the shallow and deep cumulus cases are compared and contrasted.

To derive multiscale models for deep cumulus rather than shallow cumulus, we proceed similarly to sections 2 and 3. The starting point for the models is still the dimensional Boussinesq equations in (1), but here a different set of reference scales is used to obtain the nondimensional equations for the asymptotics. While the scales of shallow cumulus parcels were used in section 2, here the scales of deep cumulus parcels are used as the basic reference scales:

$$u_{\text{ref}} = 10 \text{ m s}^{-1}, \quad x_{\text{ref}} = 1 \text{ km}, \quad \text{and} \quad t_{\text{ref}} = 100 \text{ s}.$$

These values and the pressure and heating rate values are the only reference scales that are different for the deep cumulus case, as summarized in Table 3. The thermodynamic reference scales used here are the same as they were for shallow cumulus ( $\theta_{\text{ref}} = 3.3 \text{ K}$  and  $q_{\text{ref}} = 1.3 \text{ g kg}^{-1}$ ), and the reference heating rate is then  $3.3 \text{ K (100 s)}^{-1}$ . The background stratifications are also assumed to have the same reference scales as in (2). For these new reference scales, the nondimensional number  $\epsilon = B_* = c_p \theta_0 / L_v$  keeps the same small value of  $\epsilon \approx 0.1$ , but the two nondimensional numbers  $\Gamma_*^{\theta}$  and  $\Gamma_*^q$  are now identically equal to 1.

Given these new reference scales, we can rescale the dimensional Boussinesq equations in (1) to give nondimensional equations on deep cumulus scales. The resulting equations have the same form as the

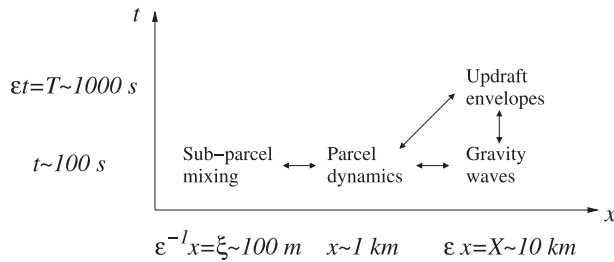


FIG. 3. As in Fig. 2, but for deep cumulus.

nondimensional equations (3) from section 2, except the  $\theta$  and  $q_v$  equations are now

$$\frac{D\theta}{Dt} + \Gamma^\theta w = C \quad \text{and} \quad \frac{Dq_v}{Dt} + \Gamma^q w = -C. \quad (27)$$

Notice the change from (3): the background stratification terms have a different apparent magnitude [i.e., they appear now as  $O(1)$  terms]. This is because their nondimensional coefficients,  $\Gamma_*^\theta$  and  $\Gamma_*^q$ , are now identically equal to 1 for deep cumulus. While each of the shallow cumulus models in sections 3 and 4 has a deep cumulus analog in this section (as summarized in Fig. 3), there will be important differences between the two cases due to the different apparent magnitude of the background stratification.

Two remarks are in order with regard to the scaling differences between shallow and deep cumulus. First, in its present form, (1) is probably an unrealistic limit for deep convection because of the absence of anelastic effects and precipitation processes; it might be relevant at best to extreme cases of pyrocumulus or the development phase of continental clouds. A Boussinesq model is used here instead of an anelastic model, not for any reason based on scaling, but for clarity of presentation. Leaving out anelastic effects helps to ease notational complexity and to ease comparison with the shallow cumulus case; in practical applications involving deep cumulus, anelastic effects should be included. Moreover, to the extent that one can generalize the treatment of the source terms, the current model provides a skeleton of a model for precipitating deep convection. Second, given the traditional notion that deep cumuli are more intense than shallow cumuli, one might be surprised that the reference heating rate used here for deep cumulus is  $O[3.3 \text{ K } (100 \text{ s})^{-1}]$ , which is smaller than the  $O[3.3 \text{ K } (30 \text{ s})^{-1}]$  heating rate used for shallow cumulus in section 3. Notice, however, that these are the heating rates on the scales of *parcels* for deep and shallow cumulus, whereas the traditional notion of intensity is likely in reference to *updraft* intensity. A comparison of the updraft-scale heating rates is, in fact,

consistent with traditional thinking: the updraft-scale heating rate for shallow cumulus was  $O[3.3 \text{ K } (300 \text{ s})^{-1}]$ , which is smaller than the  $O[3.3 \text{ K } (100 \text{ s})^{-1}]$  updraft-scale heating rate for deep cumulus, as shown below.

In summary, we have chosen a new set of reference scales for deep cumulus parcels, and we have rescaled the Boussinesq equations (1) using these reference scales. The resulting nondimensional equations look the same as (3), except for the changes to the coefficients of the background stratification terms in (27). We now proceed to look for asymptotic solutions of (27) using the small parameter  $\epsilon = B_* \approx 0.1$  with the distinguished limit of  $\Gamma_*^\theta = O(1)$  and  $\Gamma_*^q = O(1)$ .

#### a. Parcel and updraft scales

For comparison with the parcel/updraft model for shallow cumulus in section 3, we now present an analogous model for deep cumulus. The model includes interactions between deep cumulus parcels on scales of  $x_{\text{ref}} = 1 \text{ km}$  and the larger-scale updrafts on scales of  $X_{\text{ref}} = 10 \text{ km}$ . The setup for this model is identical to that in section 3, except the different moist thermodynamic equations in (27) are used and the ansatz for moisture variables in (12) is replaced by

$$q_{v,\epsilon} = \epsilon^{-1} \langle \bar{Q}_{v,d} \rangle(\epsilon \mathbf{x}, \epsilon t) + \bar{Q}_v + Q'_v + \epsilon q_v + O(\epsilon^2) \quad \text{and} \\ q_{c,\epsilon} = \epsilon^{-1} \langle \bar{Q}_{c,d} \rangle(\epsilon \mathbf{x}, \epsilon t) + \bar{Q}_c + Q'_c + \epsilon q_c + O(\epsilon^2). \quad (28)$$

The difference here is that the moisture variables are now allowed to have an  $O(\epsilon^{-1})$  contribution, which is  $O(13 \text{ g kg}^{-1})$  in dimensional units. For the scales of shallow cumulus in section 3, this  $O(\epsilon^{-1})$  moisture was not dynamic, and it appeared there simply as the background water vapor state  $\Gamma^q z$ . Also note that these  $O(\epsilon^{-1})$  moisture variables depend only on the  $O(10 \text{ km})$  deep cumulus spatial variable  $\mathbf{X}$  and are therefore labeled with a subscript  $d$ .

The equations that result from this expansion in (28) are the deep cumulus analogs of the shallow cumulus model (13)–(15) of section 3. The deep cumulus model is given by the following three sets of equations: *nonlinear parcel dynamics*,

$$\frac{D'}{Dt} \mathbf{U}' = -\nabla' P' + \mathbf{k} \Theta', \\ \frac{D'}{Dt} \Theta' + \Gamma^\theta W' = C', \\ \frac{D'}{Dt} Q'_v + \mathbf{U}' \cdot \bar{\nabla}' \langle \bar{Q}_{v,d} \rangle = -C', \\ \frac{D'}{Dt} Q'_c + \mathbf{U}' \cdot \bar{\nabla}' \langle \bar{Q}_{c,d} \rangle = C', \quad \text{and} \\ \nabla' \cdot \mathbf{U}' = 0, \quad (29)$$

where  $\nabla' = (\partial_x, \partial_y, \partial_z)$  and

$$\frac{D'}{Dt} = \partial_t + (\langle \bar{\mathbf{U}} \rangle + \tilde{\mathbf{U}} + \mathbf{U}') \cdot \nabla';$$

linear updraft pulses (now linear gravity waves),

$$\begin{aligned} \partial_t \tilde{\mathbf{U}} &= -\bar{\nabla} \tilde{P}_{-1} + \mathbf{k} \tilde{\Theta}, \\ \partial_t \tilde{\Theta} + \Gamma^\theta \tilde{W} &= \tilde{C}, \\ \partial_t \tilde{Q}_v + \tilde{\mathbf{U}} \cdot \bar{\nabla} \langle \tilde{Q}_{v,d} \rangle &= -\tilde{C}, \\ \partial_t \tilde{Q}_c + \tilde{\mathbf{U}} \cdot \bar{\nabla} \langle \tilde{Q}_{c,d} \rangle &= \tilde{C}, \quad \text{and} \quad \bar{\nabla} \cdot \tilde{\mathbf{U}} = 0, \end{aligned} \tag{30}$$

where  $\bar{\nabla} = (\partial_x, \partial_y, \partial_z)$ ; and *balanced updraft envelopes*,

$$\begin{aligned} \frac{\bar{D}}{DT} \langle \bar{\mathbf{U}}_h \rangle &= -\bar{\nabla}_h \langle \bar{P} \rangle - \bar{\nabla} \cdot \langle \bar{\mathbf{U}}' : \mathbf{U}'_h \rangle - \bar{\nabla} \cdot \langle \tilde{\mathbf{U}} : \tilde{\mathbf{U}}_h \rangle, \\ \langle \bar{\Theta} \rangle &= -\bar{\epsilon} \langle \bar{Q}_{v,d} \rangle + \langle \bar{Q}_{c,d} \rangle, \\ \Gamma^\theta \langle \bar{W} \rangle &= \langle \bar{C} \rangle, \\ \frac{\bar{D}}{DT} \langle \bar{Q}_{v,d} \rangle &= -\langle \bar{C} \rangle, \\ \frac{\bar{D}}{DT} \langle \bar{Q}_{c,d} \rangle &= \langle \bar{C} \rangle, \quad \text{and} \\ \bar{\nabla}_h \cdot \langle \bar{\mathbf{U}}_h \rangle &= -\partial_z \langle \bar{W} \rangle, \end{aligned} \tag{31}$$

where

$$\frac{\bar{D}}{DT} = \partial_T + \langle \bar{\mathbf{U}} \rangle \cdot \bar{\nabla}.$$

The derivation of these modified equations is similar to the derivation in section 3 and is not shown here in detail; one difference in the derivations is that the horizontal Helmholtz decomposition  $\mathbf{u}_h(\mathbf{x}_h, z, t) = \nabla_h \phi + \nabla_h^\perp \psi + \mathbf{b}(z, t)$  is useful here where the three-dimensional vorticity was used in section 3. Note that the balanced updraft model in (31) is identical to a model derived by Majda et al. (2010) if one ignores the interactions with processes on other scales; here the balanced updrafts interact with smaller-scale processes, whereas in Majda et al. they interact with larger-scale dynamics on mesoscales.

The deep cumulus model in (29)–(31) is different from its shallow cumulus counterpart in (13)–(15) in two main ways, and these two points support the notion that *deep cumulus dynamics are updraft dominated*, in contrast to the shallow cumulus case from section 3. First, moisture eddy flux terms are no longer leading order for the balanced updrafts in (31) because of the presence of  $O(\epsilon^{-1})$  moisture anomalies and  $O(1)$  heating anomalies on the

slow  $T$  time scale. This suggests one difference between shallow and deep cumulus: the transport of moisture is dominated by both updrafts and parcels for shallow cumulus and by updrafts alone for deep cumulus. Second, the parcel and wave equations in (29) and (30) now include large-scale gradient terms:  $\mathbf{U} \cdot \bar{\nabla} \langle \Gamma^\theta Z \rangle$ ,  $\mathbf{U} \cdot \bar{\nabla} \langle \tilde{Q}_{v,d} \rangle$ , and  $\mathbf{U} \cdot \bar{\nabla} \langle \tilde{Q}_{c,d} \rangle$ . This means that deep cumulus now feel the effects of the background stratification; therefore, instead of the updraft pulses in the shallow cumulus model in (14), deep cumuli excite gravity waves in (30). This latter difference can be seen elsewhere in previous studies: it is known that subsidence associated with deep convection occurs as a borelike gravity wave response that rapidly propagates away from the cloud (Bretherton and Smolarkiewicz 1989; Mapes 1993; Stechmann and Majda 2009), whereas subsidence associated with shallow cumulus appears in “shells” at the lateral edges of the cloud (Heus and Jonker 2008). The difference in these mechanisms of compensating subsidence is shown here to result from a difference in the apparent magnitude of the stratification on different scales.

*b. Parcel and subparcel scales*

In this section, a model is presented for the interactions between deep cumulus parcels on scales of  $x_{\text{ref}} = 1$  km and subparcel turbulent mixing on scales of  $\xi_{\text{ref}} = 100$  m. The setup for this model is identical to that in section 4, except the different moist thermodynamic equations in (27) are used. Similar to the case in section 4, note that the velocity fluctuations  $\epsilon \mathbf{u}' = O(1 \text{ m s}^{-1})$  on the new turbulent mixing scales of  $\xi_{\text{ref}} = 100$  m are still compatible with inertial-range scaling of turbulence in the atmosphere:

$$u_{\text{turb}} \approx (D \xi_{\text{ref}})^{1/3} \approx 1 \text{ m s}^{-1}.$$

The resulting equations are also nearly identical to those in section 4, except the potential temperature equations in (23), (24), and (25) now take the respective forms

$$\frac{\bar{D}}{Dt} \bar{\Theta} + \Gamma^\theta \bar{W} = \bar{C}, \tag{32}$$

$$\frac{D'}{Dt} \theta' + \mathbf{u}' \cdot \bar{\nabla} \bar{\Theta} + \Gamma^\theta w' = c', \quad \text{and} \tag{33}$$

$$\frac{\bar{D}}{Dt} \bar{\theta} + \bar{\mathbf{u}} \cdot \bar{\nabla} \bar{\Theta} + \Gamma^\theta \bar{w} = \bar{c}, \tag{34}$$

with similar changes to the water vapor equations. The derivation of these equations is essentially the same as the derivation in section 4 and is not repeated.

The main difference from the shallow cumulus case of section 4 is that the background stratification now enters

(32)–(34) at leading order. Consequently, the parcels in (32) now feel the stratification, the subparcel mixing in (33) now involves stratified turbulence, and the linear equations in (34) now support internal gravity waves.

## 6. Summary and outlook

### a. Summary

We have developed multiscale asymptotic models for different aspects of cumulus cloud dynamics. Since it is often difficult to understand how processes on different scales interact with each other, the main purpose of this paper was (i) to provide a systematic scale analysis on each scale and (ii) to clarify the nature of interactions between different scales. The presence or absence of different terms in the equations—nonlinear advection, waves, eddy flux divergence, etc.—provides insight into the dominant physical processes on each scale and across different scales. To address both detailed and general aspects, a model for shallow cumulus parcels and updrafts was discussed in detail (section 3), and the broad picture of general cumulus dynamics was discussed through two comparisons: comparison to a model for parcel and subparcel scales (section 4) and comparison to analogous models for deep cumulus (section 5).

The multiscale model in section 3 displayed a rich variety of interactions between shallow cumulus parcels and updrafts: the updrafts advect the parcels and provide an evolving background thermodynamic state for them, and, in turn, the parcels drive the updrafts through averaged condensation and eddy flux divergences. The model consists of three different, coupled dynamics for three paradigms of shallow cumulus dynamics: parcels, updraft pulses, and updraft envelopes. The updraft pulse dynamics appear to be consistent with the “pulses” seen in observations (French et al. 1999) and in simulations (Carpenter et al. 1998a; Zhao and Austin 2005; Heus et al. 2009), and we associate the updraft envelopes with the dynamics over a cloud’s lifetime, averaged over numerous parcels and pulses. The updraft envelope evolves by balanced dynamics with balance between heat sources and ascent/descent; this is a cloud-scale version of so-called weak-temperature-gradient models that have been derived for larger-scale tropical atmospheric dynamics (Sobel et al. 2001; Majda and Klein 2003; Majda et al. 2008). It was also noted that the large-scale gradients of the updrafts do not affect the parcel dynamics, whereas the parcels affect the updrafts through upscale eddy fluxes; in this sense, the model suggests that *shallow cumulus dynamics are parcel dominated*.

To complement this shallow cumulus parcel/updraft model, multiscale models were derived for other scales

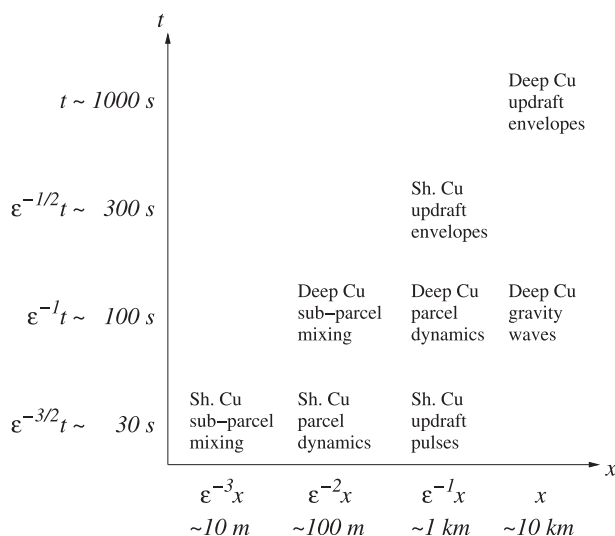


FIG. 4. The shallow and deep cumulus models and their spatial and temporal scales. For this figure only, the scale of each model is defined with respect to a single set of universal reference scales with  $x \sim 10$  km and  $t \sim 1000$  s, which are similar to the reference scales used by Klein and Majda (2006) and Majda et al. (2010).

of cumulus dynamics in sections 4 and 5, and the full set of models provides a broad overview of the similarities and differences of cumulus dynamics on different scales, which are summarized in Fig. 4. In section 4, a model was derived for the smaller scales of parcels and subparcel turbulent mixing. One important difference is that, while the parcels and updrafts operate on different time scales, the parcels and subparcel mixing share a common time scale; this is in agreement with previous work that shows that entrainment/turbulent mixing occurs on the same time scale as larger-scale cloud dynamics (Baker et al. 1984; Krueger et al. 1997; Grabowski 2007) and can significantly affect the cloud droplet spectrum (Su et al. 1998; Morrison and Grabowski 2008; Andrejczuk et al. 2009). Another difference is that the dynamical aspects of parcel/subparcel interactions are *advection dominated* in the sense that parcel-scale gradients affect the subparcel dynamics but upscale eddy fluxes do not appear at leading order.

As another comparison to the shallow cumulus case, the deep cumulus analogs of the shallow cumulus models were developed in section 5. On the one hand, shallow and deep cumulus are similar in that each shallow cumulus model has a deep cumulus analog; on the other hand, there are important differences between the shallow and deep cumulus models. The most striking difference is that the background temperature stratification is not a leading-order term for shallow cumulus, but it is a leading-order term for deep

cumulus; this leads to subsiding shells for shallow cumulus (Heus and Jonker 2008) and subsidence via bore-like gravity waves for deep cumulus (Bretherton and Smolarkiewicz 1989; Mapes 1993; Stechmann and Majda 2009). In addition, the large-scale gradients of temperature and moisture affect the parcels, but the parcels do not affect the updrafts through upscale eddy fluxes; this is the opposite of the shallow cumulus case, and it suggests that *deep cumulus dynamics are updraft dominated*.

*b. Outlook*

In addition to their use for guiding theory and interpreting simulations or observations, the models derived here also provide frameworks for multiscale numerical simulations. This is because the large and small scales of a multiscale model can be identified with resolved and unresolved scales of a numerical simulation. An example of this on larger scales in the atmosphere is superparameterization, which uses a cloud-resolving model to represent the “unresolved” convection within each “resolved” grid box of a large-scale atmospheric model (such as a general circulation model) (Grabowski 2001; Randall et al. 2003; Grabowski 2004; Majda 2007). On smaller scales, in the setting for individual clouds, a multiscale model could be used to couple resolved cloud dynamics with unresolved microphysics and turbulence, as summarized here in section 1. One challenge is to design a method to couple the resolved and unresolved processes, and the models in the present paper can be used as frameworks for this. Another challenge is to design a suitable small-scale model that allows the unresolved processes—unresolved turbulence and microphysics—to evolve dynamically and to interact with each other. The authors are currently designing such a model based on previous work (Kerstein 1991; Su et al. 1998; Kerstein 1999; Wunsch and Kerstein 2005), and results with this model will be presented elsewhere in the near future.

*Acknowledgments.* The authors thank A. Majda for helpful discussions, and they thank three anonymous reviewers for comments and suggestions that substantially improved the presentation of the paper. S. N. S. is supported by a NOAA Climate and Global Change Postdoctoral Fellowship. S. N. S. also thanks the Max-

Planck-Institut für Meteorologie, where a portion of this work was carried out, for providing visitor travel funds and accommodation.

APPENDIX

**Derivation of Shallow Cumulus Parcel/Subparcel Model**

The derivation of the parcel/subparcel model in section 4 is as follows. Upon inserting the ansatz (21) into the continuity equation of (3), the  $O(1)$  part is  $\nabla' \cdot \mathbf{u}' + \bar{\nabla} \cdot \langle \bar{\mathbf{U}} \rangle = 0$ . The spatial average of this is  $\bar{\nabla} \cdot \langle \bar{\mathbf{U}} \rangle = 0$  since  $\bar{\nabla}' \cdot \mathbf{u}' = 0$  because of the condition (11), and the spatial fluctuation at  $O(1)$  is then  $\nabla' \cdot \mathbf{u}' = 0$ , which demonstrates the derivation of the continuity equations in (23) and (24), respectively. To derive the continuity equation of (25), consider the  $O(\epsilon)$  part of the continuity equation, which is  $\nabla' \cdot \mathbf{u}'_2 + \bar{\nabla} \cdot \mathbf{u} = 0$ . Applying a spatial average to this equation and using the condition from (11) leads to the continuity equation in (25).

The derivation of the  $O(1)$  equations will be demonstrated using the potential temperature as an example; equations for the other variables follow in a similar way. Upon inserting the ansatz (21) into (3), the  $O(1)$  part of the potential temperature equation is

$$\partial_\tau \theta + \langle \bar{\mathbf{U}} \rangle \cdot \nabla' \theta = -\partial_\tau \langle \bar{\Theta} \rangle - \langle \bar{\mathbf{U}} \rangle \cdot \bar{\nabla} \langle \bar{\Theta} \rangle + \langle \bar{C} \rangle. \quad (A1)$$

The goal is to ensure sublinear growth of  $\theta$  as a function of the small-scale variables  $\xi$  and  $\tau$ . To this end, it is useful to define a change of variables on the smaller scales:

$$\xi_* = \xi - \langle \bar{\mathbf{U}} \rangle \tau \quad \text{and} \quad \tau_* = \tau. \quad (A2)$$

Physically, this puts the smaller-scale fluctuations in a reference frame moving with the larger-scale parcel. Notice that  $\mathbf{x}$  and  $t$  are regarded as frozen parameters and  $\langle \bar{\mathbf{U}} \rangle(\mathbf{x}, t)$  is thus a fixed translation speed from the perspective of the smaller scales  $\xi$  and  $\tau$ . Therefore, the derivatives with respect to the new coordinates are given by  $\partial_\xi = \partial_{\xi_*}$  and  $\partial_\tau = \partial_{\tau_*} - \langle \bar{\mathbf{U}} \rangle \cdot \nabla_*$ , where  $\nabla_* = (\partial_{\xi_*}, \partial_{\eta_*}, \partial_{\zeta_*})$ . The space and time averages here are then understood as averages in the moving reference frame and are defined as

$$\bar{f}(\mathbf{x}, t, \tau_*) = \lim_{L \rightarrow \infty} \frac{1}{(2L)^3} \int_{-L}^L \int_{-L}^L \int_{-L}^L f(\mathbf{x}, \xi_*, t, \tau_*) d\xi_* d\eta_* d\zeta_* \quad \text{and} \quad \langle f \rangle(\mathbf{x}, \xi_*, t) = \lim_{\sigma \rightarrow \infty} \frac{1}{2\sigma} \int_{-\sigma}^{\sigma} f(\mathbf{x}, \xi_*, t, \tau_*) d\tau_*, \quad (A3)$$

where fluctuations are defined as  $f' = f - \bar{f}$  and  $\tilde{f} = f - \langle f \rangle$  for a general function  $f(\mathbf{x}, \xi_*, t, \tau_*)$ . With these new coordinates, (A1) can then be rewritten as

$$\partial_{\tau_*} \theta = -\partial_t \langle \bar{\theta} \rangle - \langle \bar{\mathbf{U}} \rangle \cdot \bar{\nabla} \langle \bar{\theta} \rangle + \langle \bar{C} \rangle. \quad (\text{A4})$$

The equation for the  $O(1)$  potential temperature,  $\langle \bar{\theta} \rangle$ , is obtained by requiring sublinear growth of  $\theta$  in (A4). Notice that (A4) is an equation of the form  $\partial_{\tau_*} \theta = g(t)$ , where  $g(t)$  is independent of  $\tau_*$ , and where  $t$  is treated as a frozen parameter. For an equation of this form,  $\theta$  grows sublinearly as a function of  $\tau_*$  if and only if  $g = 0$ , which gives the parcel equation in (23). Also, if  $g = 0$ , then  $\theta$  must obey

$$\partial_{\tau_*} \theta = 0; \quad \text{that is, } \theta = \langle \theta \rangle. \quad (\text{A5})$$

The fact that the  $O(\epsilon)$  potential temperature  $\theta$  has no temporal fluctuation will be used below in the derivation of the subparcel mixing equations.

The equations for subparcel mixing come from inserting the ansatz (21) into (3) and collecting the  $O(\epsilon)$  terms, which are

$$\begin{aligned} \partial_{\tau_*} \theta_2 = & -\partial_t \langle \theta \rangle - \langle \bar{\mathbf{U}} \rangle \cdot \bar{\nabla} \langle \theta \rangle - \langle \mathbf{u} \rangle \cdot \nabla' \langle \theta \rangle \\ & - \langle \mathbf{u} \rangle \cdot \bar{\nabla} \langle \bar{\theta} \rangle - \Gamma^\theta \langle \bar{W} \rangle + c \quad \text{and} \end{aligned} \quad (\text{A6})$$

$$\begin{aligned} \partial_{\tau_*} \mathbf{u}_2 + \bar{\nabla} \bar{p}' + \nabla' p'_2 = & -\partial_t \langle \mathbf{u} \rangle - \langle \bar{\mathbf{U}} \rangle \cdot \bar{\nabla} \langle \mathbf{u} \rangle \\ & - \langle \mathbf{u} \rangle \cdot \nabla' \langle \mathbf{u} \rangle - \langle \mathbf{u} \rangle \cdot \bar{\nabla} \langle \bar{\mathbf{U}} \rangle \\ & + \mathbf{k} \langle \theta \rangle + \mathbf{k} \langle \bar{\epsilon} \langle \bar{Q}_v \rangle - \langle \bar{Q}_c \rangle \rangle, \end{aligned} \quad (\text{A7})$$

where  $\mathbf{u} = \langle \mathbf{u} \rangle$  by an argument similar to that in (A5). Note that (A6) is an equation of the form  $\partial_{\tau_*} \theta_2 = h(\tau_*, t)$ , where  $t$  is treated as a frozen parameter. For an equation of this form,  $\theta_2$  grows sublinearly as a function of  $\tau_*$  if and only if  $\langle h \rangle = 0$ , which gives (25) and (24) after splitting the result into spatial mean and fluctuating parts, respectively. The derivations of the water vapor and condensate equations are similar and are not shown in detail.

To ensure sublinear growth of  $\mathbf{u}_2$ , consider the spatial mean and fluctuating parts of (A7):

$$\begin{aligned} \partial_{\tau_*} \tilde{\mathbf{u}}_2 + \bar{\nabla} \tilde{p}' = & -\partial_t \langle \bar{\mathbf{u}} \rangle - \langle \bar{\mathbf{U}} \rangle \cdot \bar{\nabla} \langle \bar{\mathbf{u}} \rangle - \langle \bar{\mathbf{u}} \rangle \cdot \bar{\nabla} \langle \bar{\mathbf{U}} \rangle - \bar{\nabla} \langle \bar{p}' \rangle \\ & + \mathbf{k} \langle \bar{\theta} \rangle + \mathbf{k} \langle \bar{\epsilon} \langle \bar{Q}_v \rangle - \langle \bar{Q}_c \rangle \rangle, \end{aligned} \quad (\text{A8})$$

$$\bar{\nabla} \cdot \tilde{\mathbf{u}}_2 = 0, \quad (\text{A9})$$

$$\begin{aligned} \partial_{\tau_*} \tilde{\mathbf{u}}_2' + \nabla' \tilde{p}'_2 = & -\partial_t \langle \mathbf{u}' \rangle - \langle \bar{\mathbf{U}} \rangle \cdot \bar{\nabla} \langle \mathbf{u}' \rangle - \langle \mathbf{u} \rangle \cdot \nabla' \langle \mathbf{u}' \rangle \\ & - \langle \mathbf{u}' \rangle \cdot \bar{\nabla} \langle \bar{\mathbf{U}} \rangle - \nabla' \langle p'_2 \rangle + \mathbf{k} \langle \theta' \rangle, \quad \text{and} \end{aligned} \quad (\text{A10})$$

$$\nabla' \cdot \tilde{\mathbf{u}}_2' = 0, \quad (\text{A11})$$

where the incompressibility conditions can be derived from (3) by recalling that  $\mathbf{u} = \langle \mathbf{u} \rangle$ . Notice that the linear operators for  $\tilde{\mathbf{u}}_2$  and  $\tilde{p}'$  in (A8) and (A9) and for  $\tilde{\mathbf{u}}_2'$  and  $\tilde{p}'_2$  in (A10) and (A11) are the same as in the derivation in (20); thus, the remainder of the derivation here is completed as in (20).

## REFERENCES

- Albrecht, B. A., 1989: Aerosols, cloud microphysics, and fractional cloudiness. *Science*, **245**, 1227–1230.
- Andrejczuk, M., W. W. Grabowski, S. P. Malinowski, and P. K. Smolarkiewicz, 2009: Numerical simulation of cloud-clear air interfacial mixing: Homogeneous versus inhomogeneous mixing. *J. Atmos. Sci.*, **66**, 2493–2500.
- Baker, M., R. Breidenthal, T. Chouarton, and J. Latham, 1984: The effects of turbulent mixing in clouds. *J. Atmos. Sci.*, **41**, 299–304.
- Biello, J. A., and A. J. Majda, 2005: A new multiscale model for the Madden-Julian oscillation. *J. Atmos. Sci.*, **62**, 1694–1721.
- Blyth, A., 1993: Entrainment in cumulus clouds. *J. Appl. Meteor.*, **32**, 626–641.
- Bodenschatz, E., S. P. Malinowski, R. A. Shaw, and F. Stratmann, 2010: Can we understand clouds without turbulence? *Science*, **327**, 970–971.
- Bretherton, C. S., and P. K. Smolarkiewicz, 1989: Gravity waves, compensating subsidence and detrainment around cumulus clouds. *J. Atmos. Sci.*, **46**, 740–759.
- Brown, A. R., 1999: The sensitivity of large-eddy simulations of shallow cumulus convection to resolution and subgrid model. *Quart. J. Roy. Meteor. Soc.*, **125**, 469–482.
- Burnet, F., and J.-L. Brenguier, 2007: Observational study of the entrainment-mixing process in warm convective clouds. *J. Atmos. Sci.*, **64**, 1995–2011.
- Carpenter, R. L., Jr., K. K. Droegemeier, and A. M. Blyth, 1998a: Entrainment and detrainment in numerically simulated cumulus congestus clouds. Part I: General results. *J. Atmos. Sci.*, **55**, 3417–3432.
- , —, and —, 1998b: Entrainment and detrainment in numerically simulated cumulus congestus clouds. Part II: Cloud budgets. *J. Atmos. Sci.*, **55**, 3433–3439.
- , —, and —, 1998c: Entrainment and detrainment in numerically simulated cumulus congestus clouds. Part III: Parcel analysis. *J. Atmos. Sci.*, **55**, 3440–3455.
- French, J. R., G. Vali, and R. D. Kelly, 1999: Evolution of small cumulus clouds in Florida: Observations of pulsating growth. *Atmos. Res.*, **52**, 143–165.
- Grabowski, W. W., 2001: Coupling cloud processes with the large-scale dynamics using the cloud-resolving convection parameterization (CRCP). *J. Atmos. Sci.*, **58**, 978–997.
- , 2004: An improved framework for superparameterization. *J. Atmos. Sci.*, **61**, 1940–1952.
- , 2007: Representation of turbulent mixing and buoyancy reversal in bulk cloud models. *J. Atmos. Sci.*, **64**, 3666–3680.
- , and T. L. Clark, 1991: Cloud-environment interface instability: Rising thermal calculations in two spatial dimensions. *J. Atmos. Sci.*, **48**, 527–546.

- , and —, 1993a: Cloud–environment interface instability. Part II: Extension to three spatial dimensions. *J. Atmos. Sci.*, **50**, 555–573.
- , and —, 1993b: Cloud–environment interface instability. Part III: Direct influence of environmental shear. *J. Atmos. Sci.*, **50**, 3821–3828.
- Heus, T., and H. J. J. Jonker, 2008: Subsiding shells around shallow cumulus clouds. *J. Atmos. Sci.*, **65**, 1003–1018.
- , —, H. E. A. Van den Akker, E. J. Griffith, M. Koutek, and F. H. Post, 2009: A statistical approach to the life cycle analysis of cumulus clouds selected in a virtual reality environment. *J. Geophys. Res.*, **114**, D06208, doi:10.1029/2008JD010917.
- Houghton, J., Y. Ding, M. Griggs, P. Noguier, P. van der Linden, X. Dai, K. Maskell, and C. Johnson, Eds., 2001: *Climate Change 2001: The Scientific Basis*. Cambridge University Press, 881 pp.
- Houze, R., 1993: *Cloud Dynamics*. Academic Press, 573 pp.
- Kerstein, A. R., 1991: Linear-eddy modelling of turbulent transport. Part 6. Microstructure of diffusive scalar mixing fields. *J. Fluid Mech.*, **231**, 361–394.
- , 1999: One-dimensional turbulence: Model formulation and application to homogeneous turbulence, shear flows, and buoyant stratified flows. *J. Fluid Mech.*, **392**, 277–334.
- Kevorkian, J., and J. D. Cole, 1996: *Multiple Scale and Singular Perturbation Methods*. Applied Mathematical Sciences Series, Vol. 114, Springer-Verlag, 632 pp.
- Klein, R., 2000: Asymptotic analyses for atmospheric flows and the construction of asymptotically adaptive numerical methods. *Z. Angew. Math. Mech.*, **80**, 765–777.
- , 2010: Scale-dependent models for atmospheric flows. *Annu. Rev. Fluid Mech.*, **42**, 249–274.
- , and A. Majda, 2006: Systematic multiscale models for deep convection on mesoscales. *Theor. Comput. Fluid Dyn.*, **20**, 525–551.
- Krueger, S., C. Su, and P. McMurtry, 1997: Modeling entrainment and finescale mixing in cumulus clouds. *J. Atmos. Sci.*, **54**, 2697–2712.
- Madden, R., and P. Julian, 1971: Detection of a 40–50 day oscillation in the zonal wind in the tropical Pacific. *J. Atmos. Sci.*, **28**, 702–708.
- Majda, A. J., 2003: *Introduction to PDEs and Waves for the Atmosphere and Ocean*. Courant Lecture Notes in Mathematics Series, Vol. 9, American Mathematical Society, 234 pp.
- , 2007: Multiscale models with moisture and systematic strategies for superparameterization. *J. Atmos. Sci.*, **64**, 2726–2734.
- , and R. Klein, 2003: Systematic multiscale models for the tropics. *J. Atmos. Sci.*, **60**, 393–408.
- , and S. N. Stechmann, 2009: A simple dynamical model with features of convective momentum transport. *J. Atmos. Sci.*, **66**, 373–392.
- , M. Mohammadian, and Y. Xing, 2008: Vertically sheared horizontal flow with mass sources: A canonical balanced model. *Geophys. Astrophys. Fluid Dyn.*, **102**, 543–591.
- , Y. Xing, and M. Mohammadian, 2010: Moist multi-scale models for the hurricane embryo. *J. Fluid Mech.*, **657**, 478–501.
- Mapes, B., 1993: Gregarious tropical convection. *J. Atmos. Sci.*, **50**, 2026–2037.
- Moncrieff, M. W., M. Shapiro, J. Slingo, and F. Molteni, 2007: Collaborative research at the intersection of weather and climate. *WMO Bull.*, **56**, 204–211.
- Morrison, H., and W. W. Grabowski, 2008: Modeling supersaturation and subgrid-scale mixing with two-moment bulk warm microphysics. *J. Atmos. Sci.*, **65**, 792–812.
- Randall, D., M. Khairoutdinov, A. Arakawa, and W. Grabowski, 2003: Breaking the cloud parameterization deadlock. *Bull. Amer. Meteor. Soc.*, **84**, 1547–1564.
- Rogers, R., and M. Yau, 1989: *A Short Course in Cloud Physics*. Butterworth–Heinemann, 293 pp.
- Seifert, A., and B. Stevens, 2010: Microphysical scaling relations in a kinematic model of isolated shallow cumulus clouds. *J. Atmos. Sci.*, **67**, 1575–1590.
- Shaw, R., 2003: Particle–turbulence interactions in atmospheric clouds. *Annu. Rev. Fluid Mech.*, **35**, 183–227.
- Siebesma, A., and Coauthors, 2003: A large eddy simulation intercomparison study of shallow cumulus convection. *J. Atmos. Sci.*, **60**, 1201–1219.
- Sobel, A. H., J. Nilsson, and L. M. Polvani, 2001: The weak temperature gradient approximation and balanced tropical moisture waves. *J. Atmos. Sci.*, **58**, 3650–3665.
- Sommeria, G., 1976: Three-dimensional simulation of turbulent processes in an undisturbed trade wind boundary layer. *J. Atmos. Sci.*, **33**, 216–241.
- Stechmann, S. N., and A. J. Majda, 2009: Gravity waves in shear and implications for organized convection. *J. Atmos. Sci.*, **66**, 2579–2599.
- Stevens, B., 2005: Atmospheric moist convection. *Annu. Rev. Earth Planet. Sci.*, **33**, 605–643.
- , and A. Seifert, 2008: Understanding macrophysical outcomes of microphysical choices in simulations of shallow cumulus convection. *J. Meteor. Soc. Japan*, **86A**, 143–162.
- , and J.-L. Brenguier, 2009: Cloud controlling factors—low clouds. *Clouds in the Perturbed Climate System*, J. Heintzenberg and R. J. Charlson, Eds., MIT Press, 173–196.
- , and Coauthors, 2001: Simulations of trade wind cumuli under a strong inversion. *J. Atmos. Sci.*, **58**, 1870–1891.
- Stevens, D. E., A. S. Ackerman, and C. S. Bretherton, 2002: Effects of domain size and numerical resolution on the simulation of shallow cumulus convection. *J. Atmos. Sci.*, **59**, 3285–3301.
- Su, C., S. Krueger, P. McMurtry, and P. Austin, 1998: Linear eddy modeling of droplet spectral evolution during entrainment and mixing in cumulus clouds. *Atmos. Res.*, **47**, 41–58.
- Wunsch, S., and A. R. Kerstein, 2005: A stochastic model for high-Rayleigh-number convection. *J. Fluid Mech.*, **528**, 173–205.
- Xue, Y., L. P. Wang, and W. W. Grabowski, 2008: Growth of cloud droplets by turbulent collision–coalescence. *J. Atmos. Sci.*, **65**, 331–356.
- Zhao, M., and P. H. Austin, 2005: Life cycle of numerically simulated shallow cumulus clouds. Part II: Mixing dynamics. *J. Atmos. Sci.*, **62**, 1291–1310.